AUTOPHAGY
2017, VOL. 13, NO. 5, 834–853
http://dx.doi.org/10.1080/15548627.2017.1287651

Taylor & Francis
Taylor & Francis Group

BASIC RESEARCH PAPER

ATG4B contains a C-terminal LIR motif important for binding and efficient cleavage of mammalian orthologs of yeast Atg8

Mads Skytte Rasmussen[a], Stéphane Mouilleron[b], Birendra Kumar Shrestha[a], Martina Wirth[c], Rebecca Lee[b], Kenneth Bowitz Larsen[a], Yakubu Abudu Princely[a], Nicola O'Reilly[d], Eva Sjøttem[a], Sharon A. Tooze[c], Trond Lamark[a], and Terje Johansen[a]

[a]Molecular Cancer Research Group, Department of Medical Biology, University of Tromsø –The Arctic University of Norway, Tromsø, Norway; [b]Structural Biology, The Francis Crick Institute, London, UK; [c]Molecular Cell Biology of Autophagy Laboratory, The Francis Crick Institute, London, UK; [d]Peptide Chemistry Science Technology Platform, The Francis Crick Institute, London, UK

ABSTRACT

The cysteine protease ATG4B cleaves off one or more C-terminal residues of the inactive proform of proteins of the ortholog and paralog LC3 and GABARAP subfamilies of yeast Atg8 to expose a C-terminal glycine that is conjugated to phosphatidylethanolamine during autophagosome formation. We show that ATG4B contains a C-terminal LC3-interacting region (LIR) motif important for efficient binding to and cleavage of LC3 and GABARAP proteins. We solved the crystal structures of the GABARAPL1-ATG4B C-terminal LIR complex. Analyses of the structures and in vitro binding assays, using specific point mutants, clearly showed that the ATG4B LIR binds via electrostatic-, aromatic HP1 and hydrophobic HP2 pocket interactions. Both these interactions and the catalytic site-substrate interaction contribute to binding between LC3s or GABARAPs and ATG4B. We also reveal an unexpected role for ATG4B in stabilizing the unlipidated forms of GABARAP and GABARAPL1. In mouse embryonic fibroblast (MEF) *atg4b* knockout cells, GABARAP and GABARAPL1 were unstable and degraded by the proteasome. Strikingly, the LIR motif of ATG4B was required for stabilization of the unlipidated forms of GABARAP and GABARAPL1 in cells.

ARTICLE HISTORY
Received 24 June 2016
Revised 10 January 2017
Accepted 23 January 2017

KEYWORDS
ATG4; autophagy; GABARAP; GABARAPL1; LC3B; LIR; peptide arrays; X-ray structure

Introduction

Macroautophagy (hereafter referred to as autophagy) is an evolutionarily conserved pathway for lysosome-mediated degradation of cytosolic components.[1] The autophagic pathway begins morphologically with formation of a crescent shaped double-membrane structure, the phagophore,[2] which expands and wraps around the cytoplasmic content targeted for degradation closing upon itself to form the autophagosome.[3] The content may either be bulk cytoplasm or protein aggregates, specific macromolecules or organelles specifically recruited via selective autophagy receptors.[4,5] The autophagosomes may fuse with late endosomes, forming amphisomes,[6] before ultimately maturing by fusion with lysosomes.[7] Pioneering genetic studies in yeast revealed 14 AuTophaGy-related (*ATG*) genes (*ATG1* to *ATG14*) essential for autophagy.[8] The list has grown to 18 Atg proteins essential for autophagosome formation.[3] These Atg proteins are classified into 5 functional groups including: the Atg1 kinase complex, the autophagy-specific phosphatidylinositol 3-kinase complex, the Atg8–lipid- and Atg12–Atg5 conjugation systems, the Atg2-Atg18 complex and the transmembrane protein Atg9.[9] Please note that Atg8 follows yeast nomenclature in the description of proteins. In other models and species, there are several other orthologs and paralogs of yeast Atg8. However, for the sake of simplicity we use the term "Atg8-family" to denote orthologs and paralogs of yeast Atg8, in other species. Over 40 Atg proteins are now known in yeast, most of which have orthologs in higher eukaryotes.[9] Except for some regulatory components, these are conserved during evolution from yeast to man.

The mammalian Atg8-family proteins contain a ubiquitin-like core and a distinct N-terminal arm with 2 short α-helices. The mammalian orthologs of yeast Atg8 have 7 members divided into 2 major subfamilies: MAP1LC3/LC3 (microtubule-associated protein 1 light chain 3) A, B, B2 and C and GABARAP (gamma-aminobutyric acid receptor associated protein), GABARAPL1 (gamma-aminobutyric acid [GABA] A receptor-associated protein-like 1) and GABARAPL2.[10] The LC3-subfamily and GABARAP-subfamily proteins are anchored to the inner and outer membrane of the phagophore through lipidation to phosphatidylethanolamine (PE).[11,12] The Atg8-family proteins are involved in recruitment of cargo proteins,[4,5] proteins involved in the autophagy pathway, and regulatory proteins.[13] The Atg8 family is also involved in the expansion,[14] and closure of the phagophore.[15] Newly synthesized mammalian Atg8-family proteins contain a C-terminal

CONTACT Trond Lamark trond.lamark@uit.no Molecular Cancer Research Group, Department of Medical Biology, University of Tromsø - The Arctic University of Norway, 9037 Tromsø, Norway; Terje Johansen terje.johansen@uit.no Molecular Cancer Research Group, Department of Medical Biology, University of Tromsø - The Arctic University of Norway, 9037 Tromsø, Norway
Supplemental data for this article can be accessed on the publisher's website.

stretch of residues shielding a C-terminal glycine essential for lipidation. The glycine is exposed by cleavage of the LC3 and GABARAP proteins of the Atg8-family through the action of the cysteine protease ATG4, forming the active form-I variants (LC3-I and GABARAP-I).[11] Through interaction with ATG7 (E1-like enzyme), ATG3 (E2-like enzyme) and finally the ATG12–ATG5-ATG16L1 complex (E3-like), the LC3-I and GABARAP-I proteins undergo a covalent conjugation to PE, resulting in lipidated species (form-II) of the Atg8-family, tethered to the phagophore (e.g., LC3-II and GABARAP-II). ATG4 can subsequently cleave LC3-II or GABARAP-II proteins off the outer membrane, stripping the autophagosome of its coat of Atg8-family proteins and in the process restoring the LC3-I or GABARAP-I forms.[16,17]

A growing number of proteins have been shown to interact with the LC3 and GABARAP subfamilies through the sequence motif named the LC3-interacting region (LIR).[5,13,18] The core LIR motif, [W/F/Y]xx[L/I/V], is often preceded by a stretch of acidic residues.[13,19] The region immediately N-terminal to the core LIR may also harbor phosphorylatable serine or threonine residues. Phosphorylation of such residues has been shown to regulate binding of optineurin and several mitophagy receptors.[20,21] The LIR motif provides specificity for the autophagic process and can mediate binding with cargo proteins or proteins important for the regulation of autophagy.[13] Proteins harboring an LIR motif interact with proteins of the Atg8 family through interactions with the LIR docking site (LDS). The LDS consists of 2 hydrophobic pockets, which can envelop the aromatic and aliphatic residues of the LIR. Furthermore, the N-terminal arm of Atg8-family proteins is able to make electrostatic interactions with the acidic residues (if any) preceding the LIR.[13,22,23]

The mammalian Atg4-family consists of 4 different members (ATG4 isoforms A,B,C and D).[24] ATG4B, the main human ortholog, acts efficiently in both the initial cleavage and the delipidation of all proteins of the Atg8 family.[25–27] ATG4A has been shown to cleave GABARAPL2 in vitro and in vivo, but does not cleave LC3B,[26,28,29] whereas ATG4D has been reported to be important for GABARAPL1 processing in vivo following caspase-mediated activation.[30] A clear role for ATG4C has yet to be determined but a function during starvation has been reported.[31] The cleavage of Atg8-family proteins by ATG4, and subsequent conjugation to PE provide 2 opportunities for regulating autophagy. The delipidation of Atg8-family proteins by ATG4 from the autophagosomal membrane has also been suggested as a possible regulatory step, as delipidation of the Atg8 family bound to the outer membrane may function as a prerequisite for both efficient autophagosome formation and maturation.[16,32–34] Reactive oxygen species can directly inhibit the delipidating activity of ATG4A and ATG4B by oxidation of a noncatalytic residue near the active site.[35] Knockout of *Atg4b* or expression of the catalytically inactive mutant (C74S) arrests autophagy as measured by higher basal SQSTM1/p62 levels and the lack of form-II of Atg8-family proteins. On the other hand, overexpression of ATG4B also leads to arrested autophagy judged by the same measures,[36] indicating an inhibitory role for ATG4B in autophagy.

The crystal structure of both processed and unprocessed LC3B bound to a C-terminally truncated catalytically inert ATG4B has been solved.[37] In free ATG4B, the regulatory loop masks the entrance and the N-terminal tail masks the exit to the active site. Both the regulatory loop of the active site and the N-terminal tail of ATG4B undergo large conformational changes upon binding the substrate, LC3B. This exposes the active site and allows ATG4B to access membrane bound, lipidated LC3B. Consistent with a negative regulatory role deletion of the N-terminal tail increased the in vitro cleavage efficiency of ATG4B. The N-terminal tail contains a putative LIR motif that in the X-ray structures was found to interact with adjacent, nonsubstrate LC3B molecules via the LDS site. This could be part of an activation mechanism to unmask the exit of the active site.[37]

Here we show that ATG4B harbors a C-terminal LIR motif important for binding and cleavage of Atg8-family proteins with a particular role in stabilizing the unlipidated forms of GABARAP and GABARAPL1. Crystal structures of the complex of GABARAPL1 with 2 LIR peptides at 1.55- and 1.75-Å resolution reveal canonical LIR-LDS interactions with important contributions from electrostatic interactions involving residues both N-terminal to, and within, the core LIR.

Results

ATG4B contains a C-terminal LIR motif important for a strong interaction with Atg8-family orthologs

We have previously identified functional LIR motifs preferentially interacting with GABARAP subfamily proteins in ULK1 and ULK2, ATG13 and RB1CC1 of the human ULK complex.[19] Hence, we asked if other important regulatory components of the autophagy machinery, in particular the LC3- and GABARAP-activating protease ATG4B contained functional LIR motifs. In an unbiased approach we used the iLIR[38] server to predict LIR motifs, and a peptide array screen to map GABARAP-binding motifs in human ATG4B. iLIR returned 3 top hits, 2 of which reside at the extreme N- and C-termini which are predicted to be disordered by the PONDR-FIT algorithm (Fig. 1A).[39] Strikingly, the peptide array (overlapping 20-mer peptides shifted by a window of 3 amino acids along the entire sequence of ATG4B) also identified the same 3 putative LIR motifs; a putative N-terminal LIR motif (YDTL), another putative motif (FELV) just C-terminal to the protease domain, and a third motif (FEIL) located in the very C terminus (Fig. 1B).

The published crystal structure for a C-terminally truncated ATG4B and full-length LC3B reveals an interactions mainly located around the active site of ATG4B (C74) with the critical C-terminal glycine of LC3B interacting with these residues.[37] Regarding the putative LIRs we identified, the side chains of the FELV motif are hidden in the reported crystal structure, suggesting that it may not act as a functional LIR motif in the full-length protein. However, as the YDTL and the FEIL are both placed in disordered regions of ATG4B (Fig. 1A), they are more likely to engage in interactions with Atg8-family proteins. Interestingly, the C-terminal FEIL LIR motif clearly displayed the strongest binding to GST-GABARAP. Notably, a weak interaction was also observed with a peptide containing only the first 2 residues of the core LIR motif (Fig. 1B). The N-

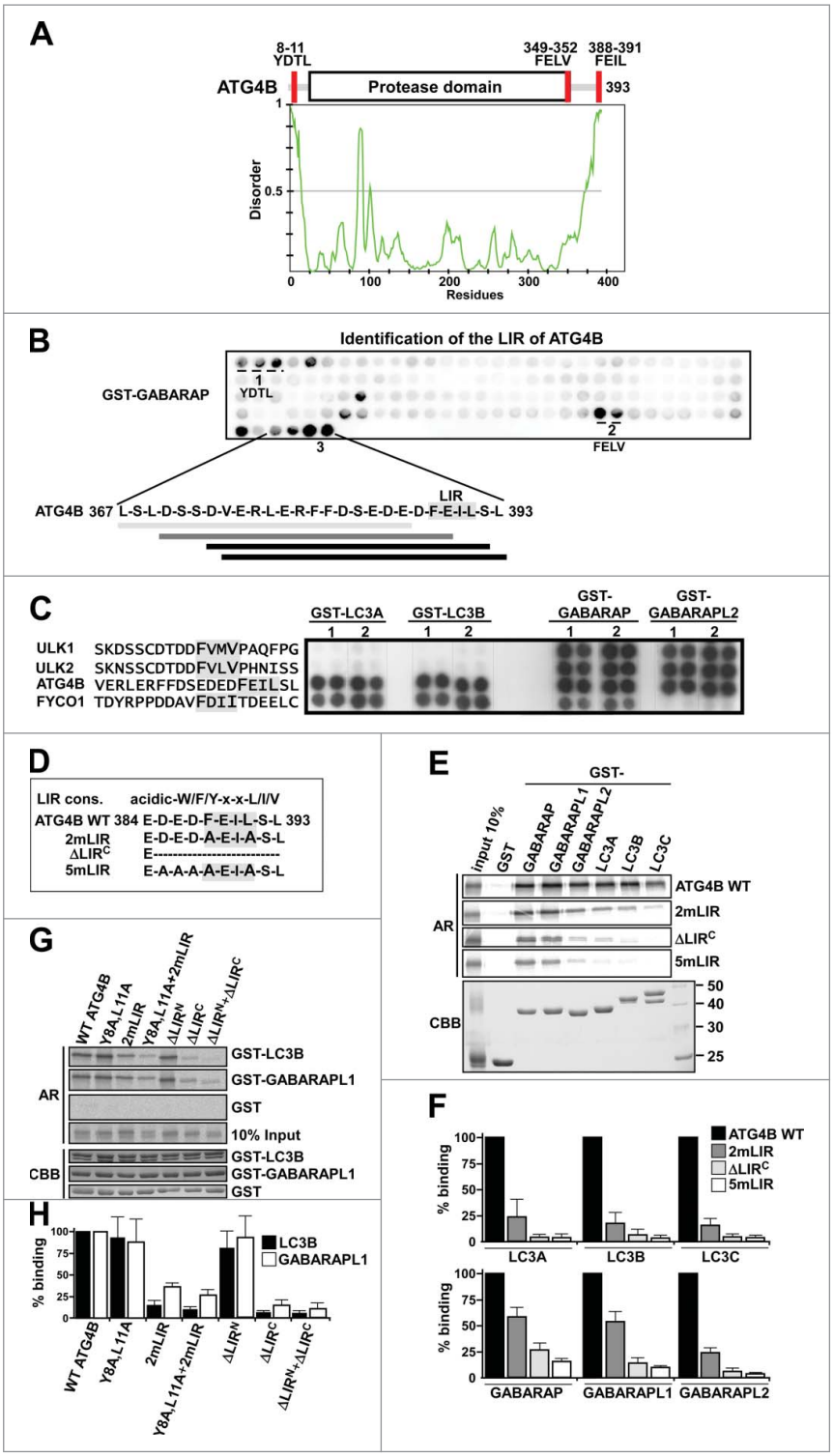

Figure 1. ATG4B contains a C-terminal LIR motif important for a strong interaction with Atg8-family orthologs. (A) Schematic overview of ATG4B indicating disordered regions and LIR motifs predicted by the iLIR and PONDR-FIT servers. (B) Identification of a C-terminal LIR motif. An array of 20-mer peptides covering full-length ATG4B (each peptide shifted 3 amino acids relative to the previous) was mixed with GST-GABARAP (1 μg/ml) and binding detected with GST antibodies. The extension of the most strongly interacting peptides is indicated below in black. (C) The C-terminal LIR in ATG4B interacts with the LC3 and GABARAP subfamilies. The indicated peptides from ULK1, ULK2, ATG4B and FYCO1 (synthesized in duplicates marked 1 and 2) were examined as in B in a peptide array for binding to GST-tagged Atg8-family orthologs. (D) C-terminal sequences of ATG4B constructs carrying mutations affecting the C-terminal LIR motif. (E) The C-terminal LIR motif is important for the interaction of full-length ATG4B with Atg8-family orthologs. Myc-tagged ATG4B constructs were in vitro translated in the presence of [^{35}S]methionine, and tested in GST affinity isolation experiments for binding to the indicated Atg8-family orthologs fused to GST. Bound proteins were detected by autoradiography (AR), and immobilized GST or GST-tagged proteins by Coomassie brilliant blue staining (CBB). (F) Quantification of E, % binding relative to WT ATG4B based on 3 independent experiments. (G) A putative N-terminal LIR is not important for the interaction of ATG4B with LC3B or GABARAPL1. MYC-tagged ATG4B constructs were in vitro translated and tested for binding to GST-LC3B and GST-GABARAPL1 as in (E). (H) Quantification of (G) from 3 independent experiments.

terminal YDTL and the internal FELV LIR motifs displayed a weaker interaction with GST-GABARAP (Fig. 1B). Note, in the reported structure of the ATG4B-LC3B complex,[37] the N-terminal YDTL motif is bound at the LIR docking site (LDS) of a LC3B molecule adjacent to the LC3B molecule bound to the active site of ATG4B.

The strong GABARAP interaction with the C-terminal LIR in ATG4B prompted us to focus on this unstudied LIR motif. To determine its specificity for the various Atg8-family proteins, we first tested a peptide containing this LIR for interaction with GST-LC3A, GST-LC3B, GST-GABARAP and GST-GABARAPL2 (Fig. 1C). A strong interaction was observed with all 4 members of the Atg8 family, indicating the C-terminal LIR has a broad specificity. Next, a series of mutant ATG4B constructs, either deleted for the C-terminal LIR region (ΔLIR^{C}) or carrying 2 (2mLIR) or 5 (5mLIR) point mutations affecting the motif (Fig. 1D), were in vitro translated and tested for interaction with Atg8-family orthologs fused to GST. Mutation of 2 residues in the core LIR^{C} motif (F388A and L391A) reduced the interaction of ATG4B with LC3A, LC3B, LC3C and GABARAPL2 to 25% residual binding, and the interactions with GABARAP or GABARAPL1 to 60% (Fig. 1E and F). However, mutation of 5 residues in the LIR^{C} region, or deletion of the LIR^{C} motif, reduced the interactions with GABARAP and GABARAPL1 to 10% to 15% (Fig. 1E and F). The 5 point-mutations included the 3 negatively charged residues located immediately N-terminal to the core LIR^{C} motif (Fig. 1D), in addition to the F388A and L391A mutations. In contrast to mutation of the C-terminal LIR, mutation or deletion of the N-terminal YDTL LIR (LIR^{N}) had only a very minor effect on the interaction with LC3B or GABARAPL1 (Fig. 1G and H). Thus, we identified a LIR motif in the C terminus of ATG4B that contributed strongly to the interaction between ATG4B and Atg8-family proteins. The finding that LIR^{N} of ATG4B is not important for the interaction is entirely consistent with published structural data showing that the catalytic core of ATG4B and LIR^{N} interact with 2 adjacent LC3B molecules.[37] We propose that the LIR in the C terminus of ATG4B strongly increases the affinity of the interaction because it can adopt a cis-type interaction where the catalytic core and this LIR interact with the same Atg8-family molecule.

Structure of the GABARAPL1-ATG4B LIR^{C} complex

To evaluate the interaction between the C-terminal LIR-motif of ATG4B with Atg8-family proteins in more detail, we determined the X-ray structure of GABARAPL1 in complex with a peptide containing the C-terminal 10-amino acid LIR^{C} motif of ATG4B (Fig. S1A). The crystal structure of the ATG4B peptide-bound GABARAPL1 is similar to the previously reported structures of GABARAPL1 alone (PDB code 2PQR) and GABARAPL1 in complex with the LIR of NBR1.[40] These structures have an average 0.74 and 0.78 Å root mean square deviation for the C-α positions, respectively. ATG4B C-terminal FEIL LIR binds GABARAPL1 in an extended conformation with the core residues ATG4B (F388) and ATG4B (L391) deeply bound into the 2 hydrophobic pockets HP1 and HP2, as described previously for canonical LIR interactions (Fig. 2A).[13] The structure displays 4 additional interactions: 1) Electrostatic interactions between the acidic N-terminal LIR^{C} residues ^{384}Glu-Asp-Glu-Asp^{387} of ATG4B and the basic residues GABARAPL1 (K46), GABARAPL1 (K24), GABARAPL1 (K20) and GABARAPL1 (K48), respectively; 2) a salt bridge between ATG4B (E389) and GABARAPL1 (R67); 3) some hydrophobic interactions between ATG4B (I390) in position +2 and GABARAPL1 (L50) as well as GABARAPL1 (Y25); 4) 3 hydrogen bonds between the carbonyls of ATG4B (L391), ATG4B (S392) and the guanidinium group of GABARAPL1 (R28). Except for the C-terminal ATG4B (L393), all residues in the LIR^{C} are contributing to the interaction. Two sulfate ions are bound to the basic grove formed between GABARAPL1 N-terminal arm (helix α1 and α2) and the β strand β2 (Fig. 2A and D). This basic patch is reported to interact with the N-terminal acidic residues of LIR motifs.[13] Hence, the presence of sulfate ions might therefore interfere with ATG4B LIR^{C} binding to GABARAPL1 under these crystallization conditions. Phosphorylation of S392, located just C-terminal to the core FEIL LIR^{C} motif of ATG4B (Fig. 1A to D), is recently reported to increase cleavage of LC3B.[41] To evaluate the importance of this phosphorylation for its interaction with the Atg8-family proteins, the X-ray structure of GABARAPL1 bound to the ATG4B LIR^{C} peptide phosphorylated on residue S392 of ATG4B(hereafter referred to as phosphorylatedATG4B LIR^{C}) (Fig. 2B and Fig. S1B) was solved. Interestingly, the N-terminal acidic amino-acids of phosphorylated ATG4B LIR^{C} interact with the basic patch of GABARAPL1 where the sulfate anions were binding in the wild-type GABARAPL1-ATG4B LIR^{C} complex (Fig. 2C and D). Indeed, ATG4B (E386) forms an important electrostatic interaction with GABARAPL1 (H9) and GABARAPL1 (R47), while the rest of the LIR^{C} binds similarly except for the phospho-serine 392 (p-S392), which points toward the solvent, and is not engaged in any contact with GABARAPL1 (Fig. 2B and C). This complex crystalized in absence of ammonium sulfate and is therefore very likely more physiological representative for the interactions of the ATG4B residues $_{384}$Glu-Asp-Glu-Asp$_{387}$. The residues GABARAPL1 (H9) and GABARAPL1 (R47) binding to ATG4B (E386) are conserved in all GABARAP isoforms but not in LC3 proteins (Fig. 2E). Similarly, arginine residue GABARAPL1 (R28) observed in all GABARAP isoforms is a lysine in all LC3 isoforms. The shorter lysine side chain may not be able to engage in an interaction similar to the arginine GABARAPL1 (R28) (Fig. 2C and E). These differences may provide an explanation for the stronger binding of ATG4B LIR^{C} to GABARAP isoforms compared with LC3 isoforms.

Interestingly, ATG4B (F388) adopts different conformations in the 2 structures. In the ATG4B LIR^{C}-GABARAPL1 complex the 2 sulfate anions form a network of hydrogen bonds with the GABARAPL1 (K48) side chain (Fig. 2D). GABARAPL1 (K48) is a key component of the hydrophobic pocket HP1 critical for the binding of the aromatic hydrophobic residue F/W/Y in position 0 of a LIR motif.[42] GABARAPL1 (K48) is usually adopting an extended conformation and is held in place by a hydrogen bond with the GABARAPL1 (E17) side chain to form one side of the HP1 (Fig. 2D and S2). GABARAPL1 (K48) adopts this conformation in complex with the phosphorylated ATG4B LIR^{C}. However, in the complex between GABARAPL1 and wild-type ATG4B LIR^{C}, GABARAPL1

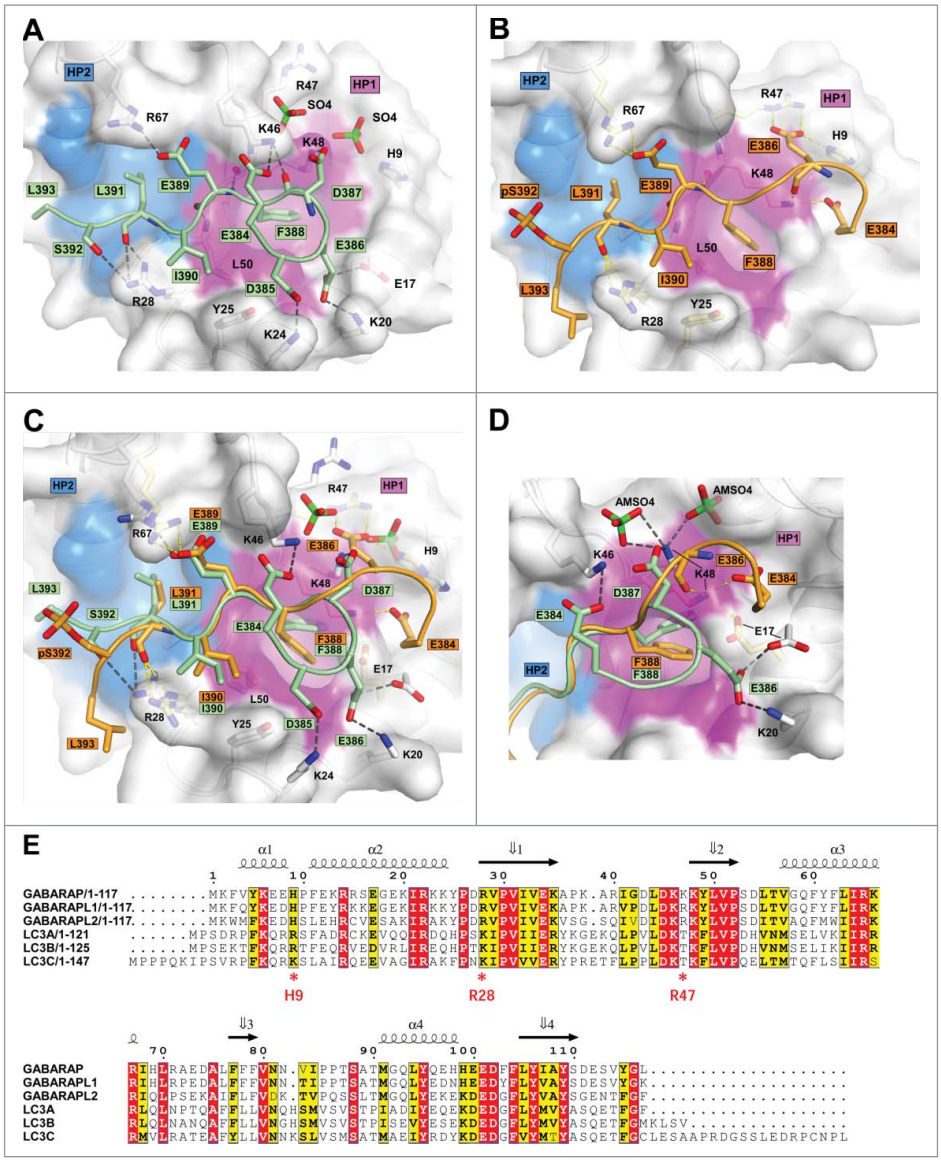

Figure 2. Structure of the GABARAPL1-ATG4B LIR^C complex. (A) Close-up of structure for wild-type ATG4B LIR^C motif bound to GABARAPL1. The LIR^C of ATG4B (amino acids 384 to 393) is displayed in green cartoon with the interacting residues shown as sticks. GABARAPL1 is displayed in white cartoon and transparent surface with the hydrophobic pocket 1 and 2 colored in pink and blue surfaces, respectively. (B) Close-up of structure of p-S392 (phosphorylated) ATG4B LIR^C motif bound to GABARAPL1. The phosphorylated LIR^C peptide (amino acids 384 to 393) is displayed in orange cartoon with the interacting residues shown as sticks. GABARAPL1 is displayed in white cartoon and transparent surface with the hydrophobic pocket 1 and 2 colored in pink and blue surfaces, respectively. (C) Superposition of the wild-type and (S392)-phosphorylated LIR^C peptide bound to GABARAPL1. Both structures are colored according to A and B. For clarity, only the surface of GABARAPL1 for the p-S392 (phosphorylated) LIR^C is displayed. (D) Same as (C). Close-up view of the hydrophobic pocket 1 in both structures. Some sidechains were removed for clarity. (E) Sequence alignment of human Atg8-family orthologs generated with ESPript 3.0.[56] Identical and similar residues are boxed in red and yellow, respectively. Red asterisks indicate key residues discussed in the text.

(K48) is engaged in multiple hydrogen bonds with the 2 sulfate anions and point in the opposite direction, widening HP1 and allowing ATG4B (F388) to adopt a more "closed" conformation (Fig. 2D and S2A and B).

The C-terminal LIR in ATG4B relies both on electrostatic interactions, as well as aromatic and hydrophobic pocket interactions for efficient binding

To analyze the relative importance of the residues encompassing the C-terminal LIR of ATG4B, 2-dimensional peptide array analyses were performed.[19] Each position of an 18-mer C-terminal ATG4B peptide was substituted with all 19 alternative amino acids and the arrays were probed for interaction with GST-LC3B and GST-GABARAPL1 (Fig. 3A). The results clearly support the presence of a canonical LIR motif in the C terminus of ATG4B. This was particularly evident when the array was probed with LC3B. Only aromatic residues are tolerated at position 0 and only hydrophobic ones at positon +3. Interestingly, the interaction with GABARAPL1 seems to be unusually tolerant to substitutions of the aromatic and hydrophobic residues in the core LIR^C motif, and in particular mutations affecting the hydrophobic L391 at position +3 (Fig. 3A). This is consistent with the results of the GST affinity isolation experiments of the 2mLIR (F388A,L391A) mutant of full-length ATG4B versus GABARAP and GABARAPL1 where only a 40% to 50% reduction in binding was seen

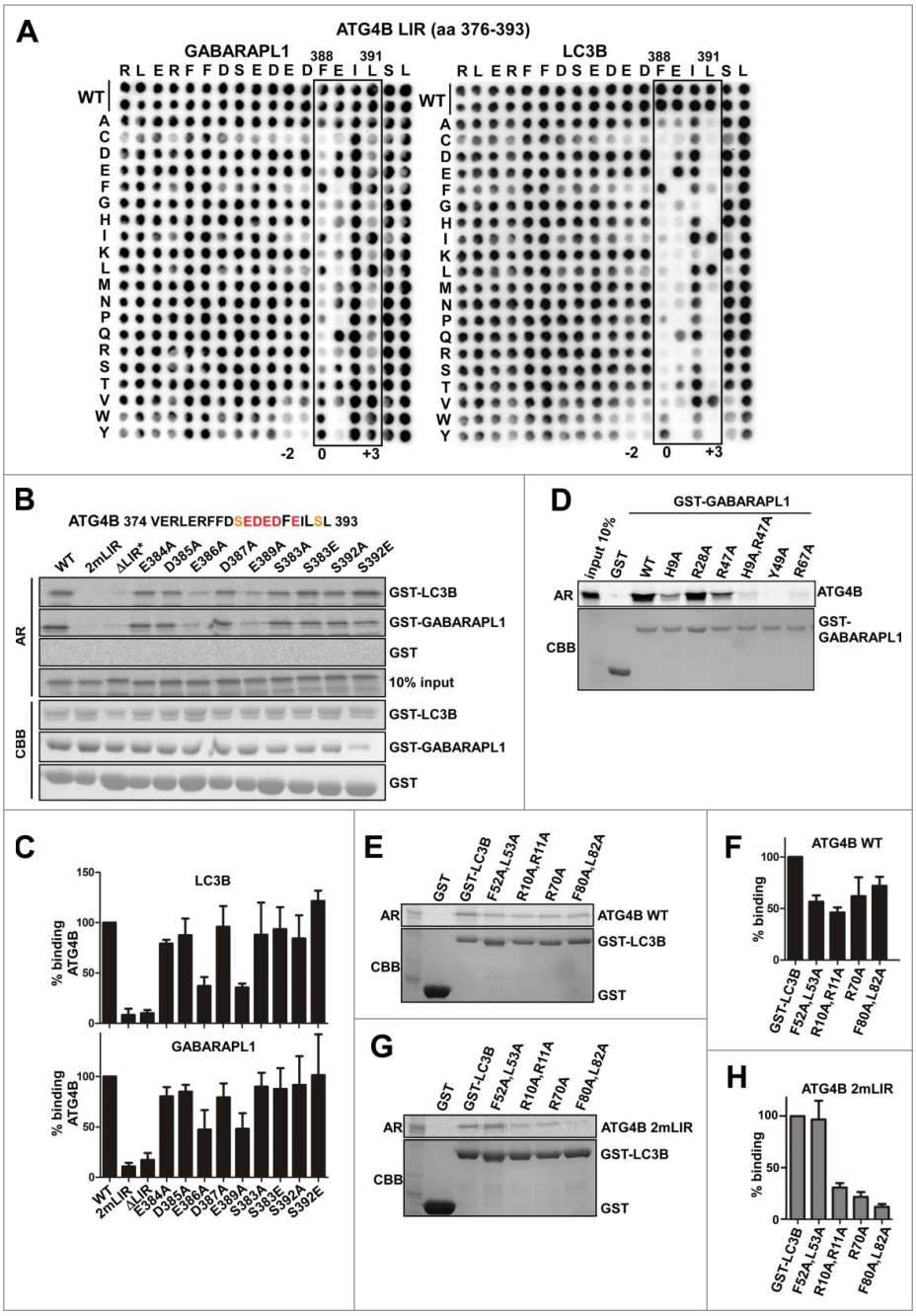

Figure 3. The C-terminal LIR in ATG4B relies both on electrostatic interactions, as well as aromatic and hydrophobic pocket interactions for efficient binding. (A) Two-dimensional peptide array scan analyzing the effects of single amino acid substitutions at all positions of the indicated 20-mer peptide from the C terminus of ATG4B. Arrays were probed with GST-GABARAPL1 or GST-LC3B. (B) E386 and E389 in the LIR^C of ATG4B form important electrostatic interactions with both LC3B and GABARAPL1. A C-terminal ATG4B peptide (amino acids 374 to 393), fused to GFP and carrying the indicated point mutations, were in vitro translated and tested in GST affinity isolation assays for binding to LC3B and GABARAPL1. The ΔLIR^C construct is indicated with an asterisk because it comprises amino acids 365 to 384 of ATG4B (LNLSLDSSDVERLERFFDSE) and 2mLIR harbors the F388A and L391A double mutation of the canonical aromatic and hydrophobic core LIR^C residues. (C) Quantification of the experiment shown in B, based on 3 independent experiments. The binding to the WT peptide is set to 100%. (D) H9 and R47 are crucial for binding of GABARAP or GABARAPL1 to the ATG4B LIR^C. The C-terminal ATG4B peptide (amino acids 374 to 393), fused to GFP was in vitro translated and tested in GST affinity isolation assays for binding to specific point mutants of GABARAPL1 fused to GST and bound to GST beads. ((E)and G) Both LIR^C-LDS interactions and catalytic site-substrate interactions contribute to ATG4B-LC3B binding. MYC-ATG4B (E) and MYC-ATG4B 2mLIR (G) were in vitro translated and tested in GST affinity isolation assays for binding to GST-LC3B with or without mutations affecting the LIR^C-LDS interaction (F52A and L53A, R10A and R11A, as well as R70A) or the catalytic site-substrate interaction (F80A and L82A). (F) Quantification of (E), the % binding relative to the binding of WT GST-LC3B to WT ATG4B based on 3 independent experiments. (H) Quantification of (G), % binding relative to the binding of WT GST-LC3B to ATG4B 2mLIR based on 3 independent experiments.

(Fig. 1E and F). Notably, the +1 position of ATG4B LIR^C is the second most vulnerable to mutations for GABARAPL1 binding. Here, substitution of E389 in the +1 position to N, D, Q, S, T and A does not impair binding, while all other substitutions decrease binding. Any amino acid can be placed in the +2 position. Aromatic and hydrophobic residues are counterselected at the −1 and −2 positions (Fig. 3A). For the ATG4B LIR^C interaction with GST-LC3B we see a classical binding pattern where substitutions of the core LIR amino acids strongly affect the binding. Only the

F and Y in the 0 position, and I, V and L in the hydrophobic +3 position are tolerated for significant binding (Fig. 3A). The negatively charged E389 at position +1 is critical also for the interaction with LC3B. Any other amino acid in this position negatively affects the interaction. Mutations of residues outside the core LIR^C have a very similar effect on LC3B and GABARAPL1 binding, including the counterselection of aromatic or hydrophobic substitutions at positions −1 and −2. However, the LC3B interaction is additionally intolerant to aromatic or hydrophobic substitutions affecting S392 at position +4.

The single point mutations were further analyzed by GST affinity isolation assays in which the C terminus of ATG4B (amino acids 373 to 393) fused to GFP was in vitro translated and tested for interaction with GST-LC3B or GST-GABARAPL1 (Fig. 3B and C). For selected single point mutants, the effect on the full-length ATG4B interaction was additionaly tested (Fig. S3). We chose to use the C-terminal ATG4B fragment in this assay, since the effects of single point mutations on the LIR^C interactions are more easily detected when there is no compensatory catalytic site interaction. The 2mLIR (F388A,L391A) double mutation strongly inhibited the interaction of the C-terminal ATG4B fragment with GST-GABARAPL1 and GST-LC3B (about 10% residual binding) (Fig. 3B and C).

To identify important acidic residues in the ATG4B LIR^C, the effect of single point mutations affecting negatively charged residues within the core ATG4B LIR^C motif (E389) or N-terminal to the core ATG4B LIR^C motif (E384, D385, E386, D387) were analyzed. The E386A (−2) and E389A (+1) mutations strongly reduced binding of the LIR^C peptide of ATG4B to both GST-LC3B and GST-GABARAPL1 (Fig. 3B and C), although their effect was less pronounced when tested in full-length ATG4B (Fig. S3). This is entirely consistent with the crystal structure showing the electrostatic interactions between ATG4B (E389) and GABARAPL1 (R67) as well as between ATG4B (E386) and GABARAPL1 (H9 and R47) (Fig. 2). The crucial roles of these electrostatic interactions for binding was also shown by GST affinity isolation assays where Ala (A) substitutions of H9, R47 and R67 abolished the binding of GABARAPL1 to the ATG4B LIR^C (Fig. 3D). The R28A mutation did not have any effect (Fig. 3D). This is consistent with the modest effect of mutating the core LIR^C hydrophobic Leu residue for binding to GABARAPL1 (Fig. 3A).

Cleavage of LC3B by ATG4B has been recently reported to be regulated by phosphorylation of S383 and S392.[41] These residues flank the core LIR^C region. We therefore analyzed the effect of mutations of S383 or S392 to alanine (A) or glutamic acid (E) on the binding of the LIR^C fragment and full-length ATG4B to GST-GABARAPL1 or GST-LC3B. None of these mutations affected the LIR^C interactions significantly. However, the S392E mutation increased binding between the ATG4B LIR^C fragment and LC3B by 20% (Fig. 3B and C). The S392E mutation also had a weak, although not significant, positive effect on the interaction of full-length ATG4B with LC3B (Fig. S3).

Both catalytic site-substrate interactions and LIR-LDS interactions contribute to the binding between LC3B and ATG4B

The ATG4B-LC3B crystal structure revealed that the F80 and L82 residues in LC3B are important for ATG4B binding and processing.[37] The LC3B surface involved in this catalytic interaction is distinct from the LDS involved in the LIR interaction.[37] To analyze the relative importance of the catalytic site interaction for binding, selected mutants of LC3B located on different binding surfaces were tested in GST affinity isolation assays for binding to WT ATG4B. We found that the F80A and L82A double mutation (affecting the catalytic site interaction) had a negative effect on ATG4B binding comparable to mutations affecting the LIR^C interaction (Fig. 3E and F). This strongly supports the conclusion that catalytic site-substrate interaction and the LIR-LDS interaction both contribute to the binding between ATG4B and LC3B. When the same experiment was repeated with the 2mLIR mutant of ATG4B, the F52A and L53A LDS mutation in LC3B had no effect (Fig. 3G and H). This is as expected since the 2mLIR mutation and the F52A and L53A double mutation both impair the hydrophobic LIR-LDS interactions. However, LC3B mutations affecting electrostatic LIR-LDS interactions or the catalytic site-substrate interaction, all strongly impaired the interaction between ATG4B 2mLIR and LC3B (Fig. 3G and H). This corroborates the dual importance of catalytic site-substrate interactions and LIR^C-LDS interactions for binding. The strong effect of the R10A and R11A double mutation is also notable, since it supports an important role for the N-terminal arm of LC3B in stabilizing the LIR^C-LDS interaction.

Theoretically, the C-terminal LIR-LDS interaction may act both in *cis* and *trans*. To investigate whether the cis interaction is sterically hindered, the structure of the phosphorylated ATG4B LIR^C motif bound to GABARAPL1 was superposed on the ATG4B (1 to 354)-LC3B complex (PDB ID: 2ZZP) to generate a model of full-length ATG4B bound to LC3B (Fig. 4A and Fig. S4). The model clearly supports that a *cis*-mediated LIR-LDS interaction is possible.

The ATG4 family shows differential binding to LC3B and GABARAP

The C-terminal LIR (FEIL) found in ATG4B is completely conserved in ATG4A, while the other 2 human ATG4 orthologs have the sequences ATG4C (FVLL) or ATG4D (FVFL) (Fig. 4B and C). When tested in GST affinity isolation assays, in vitro translated ATG4A interacted strongly with GST-LC3B and GST-GABARAP, and both interactions were strongly impaired by a deletion of the C-terminal LIR motif (Fig. 4D and E). The C terminus is only partially conserved in ATG4C and ATG4D. In these proteins, the critical acidic residue in position +1 is substituted with a hydrophobic V and the core LIR motif has no C-terminal extension (Fig. 4C). When tested in GST affinity isolation assays, these proteins interacted well, but more weakly than ATG4B, with GST-GABARAP. However, they displayed a very weak interaction with LC3B. Deletion of the C terminus had a negative effect on interactions

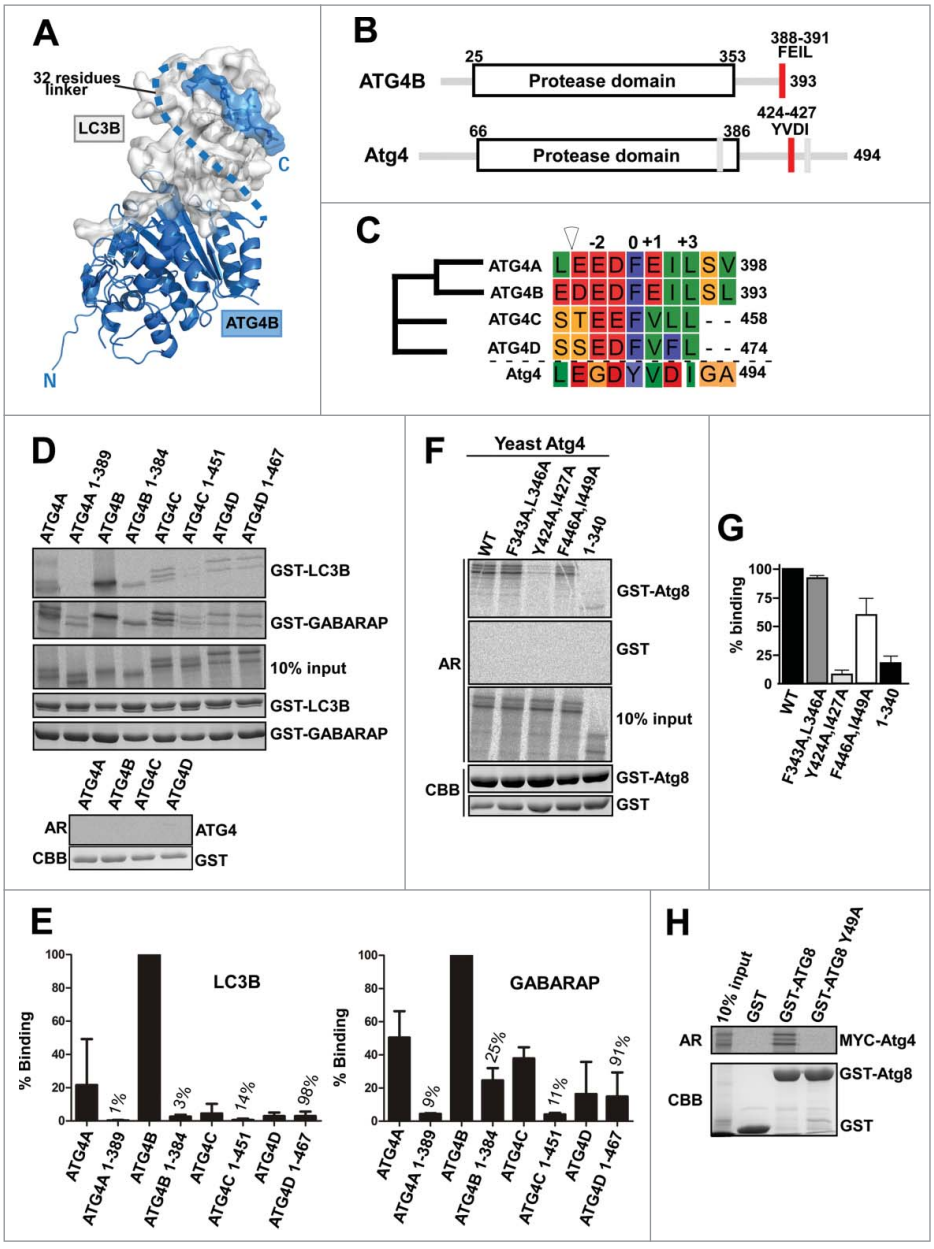

Figure 4. ATG4A and ATG4B harbor a C-terminal LIR, binding efficiently to LC3B and GABARAP, while ATG4C and ATG4D do not. (A) Model of full-length ATG4B bound to LC3B. The structure of the phosphorylated ATG4B LIR^{C} motif bound to GABARAPL1 was superposed to the ATG4B (1 to 354)-LC3B complex (PDB ID: 2ZZP) to generate a model of the full-length ATG4B bound to LC3B. ATG4B is displayed in blue cartoons and LC3B is displayed in white cartoons and transparent surface. The 32 missing residues connecting ATG4B C-terminal LIR motif to Q354 are represented by a dashed line. (B) Schematic illustration of human ATG4B and yeast Atg4 indicating the protease domain and the functional LIRs (red bar) with the location of 2 candidate LIRs in yeast Atg4 tested in F indicated as gray bars. (C) A phylogenetic tree (left), and alignment of the far C-terminal sequence of the 4 different mammalian ATG4s and yeast Atg4 LIR (referred to in yeast as the Atg8-interacting motif). (D) MYC-tagged human ATG4 orthologs (WT and LIR^{C}-deleted) were in vitro translated and tested in GST affinity isolation assays for binding to GST-LC3B and GST-GABARAP. The region deleted in the LIR^{C}-deleted constructs is indicated by an open arrowhead in (C). The affinity isolation with the respective GST controls is shown below. (E) Quantification of the experiment shown in (D), based on 3 independent experiments. Bars indicate relative binding, and the interaction with ATG4B is set to 100%. For LIR^{C}-deleted constructs, % binding relative to the corresponding full-length construct is indicated. (F) Yeast Atg4 has predicted LIR motifs binding to yeast Atg8 at a similar C-terminal distance to the protease domain as human ATG4B. Yeast Atg4 (WT and candidate LIR mutants) were in vitro translated and analyzed by GST affinity isolation assays for binding to GST-Atg8 (yeast). (G) Quantification of the experiment shown in (F), based on 3 independent experiments. WT was set to 100% binding. (H) Yeast MYC-tagged Atg4 was in vitro translated and analyzed by GST affinity isolation assays for binding to GST-Atg8 (WT and LDS mutated).

mediated by ATG4C, but it did not affect interactions mediated by ATG4D (Fig. 4D and E). Hence, the canonical LIR motif in the C terminus of ATG4B is conserved also functionally in ATG4A, while the more divergent motifs in ATG4C and ATG4D play a minor, or no, role in the binding to LC3B and GABARAP. To check for evolutionary conservation of the LIR-mediated interaction between ATG4 and the Atg8 family we looked at yeast (*S. cerevisiae*). By mutagenesis of 3 candidate LIR motifs (mutating the aromatic HP1 and hydrophobic HP2 residues to Ala) we identified a single LIR motif (YVDI; Fig. 4C) crucial for binding to yeast Atg8 (Fig. 4F and G). Although not at the extreme C terminus, strikingly, this motif is located in a similar distance C-terminal to the protease domain as the LIR motif in ATG4B (Fig. 4B). Mutation of LDS in yeast Atg8 (Y49A) abolished the interaction between yeast Atg8 and yeast Atg4 (Fig. 4H), further supporting the

conclusion that the LIR interaction is essential for binding also in yeast.

The C-terminal LIR motif of ATG4B is important for efficient cleavage of Atg8-family proteins in vitro and in vivo

The importance of the LIR^C motif for ATG4B-mediated cleavage was tested in an in vitro cleavage assay using recombinant proteins. Hence, WT, ΔLIR^C or catalytically inactive (C74S) ATG4B was added to GABARAP or LC3B fused to a C-terminal GST tag. Cleavage was measured as reduction in the amount of the full-length fusion protein. WT ATG4B had the highest cleavage activity, while only a partial cleavage was seen with ATG4B ΔLIR^C. During the 1-h time frame of the experiment, no cleavage activity was measured for the catalytically inactive ATG4B (C74S) mutant (Fig. 5A).

To analyze the effect of ATG4B C-terminal LIR mutants in cells, we established stable cell lines expressing GFP-tagged ATG4B WT, catalytic inactive C74S- or LIR^C mutants. *atg4b* knockout (KO) mouse embryo fibroblasts (MEFs)[43] were stably reconstituted with WT or the selected mutants of ATG4B using a doxycycline inducible retroviral vector. The induced expression levels of the various GFP-ATG4B fusion proteins were similar. All constructs were expressed at a low level in uninduced cells due to promoter leakage (Fig. 5B and Fig. S5A). The expression level of GFP-ATG4B without induction was 5-fold higher than that of endogenous ATG4B (Fig. S5B). It has been shown that overexpression of ATG4B inhibits lipidation of Atg8-family orthologs by preventing their delivery to ATG7.[36] Hence, we chose to use the uninduced cell lines for our experiments. To probe the requirements for ATG4B-mediated cleavage of Atg8-family proteins in cells, we used transiently transfected LC3B and GABARAPL1 fused to ACTB and Gaussia luciferase (Fig. 5C). Cleavage is measured by assaying the activity of Gaussia luciferase released into the growth medium following *in cellulo* cleavage.[44] Cells expressing WT ATG4B clearly displayed more effective cleavage (measured 18 to 24 h after transfection) than cells expressing ATG4B ΔLIR^C or 5 point mutations in the LIR motif (5mLIR). Cells expressing ATG4B (C74S) showed background levels (Fig. 5C). Strikingly, this was also the case when a LDS mutated (F52A and L53A) LC3B was used as reporter (Fig. 5C). Taken together, these results strongly support our finding that the LIR^C interaction is important for efficient cleavage by ATG4B.

To compare the relative importance of the N-terminal and C-terminal LIR motifs in ATG4B for cleavage, another series of *atg4b* KO MEFs stably reconstituted with selected ATG4B mutants fused to GFP were made (Fig. 5D). Reconstituted cells were transiently transfected with LC3B and GABARAPL1 fused to ACTB and Gaussia luciferase, and assayed for *in vivo* cleavage activity. Deletion of the N-terminal LIR (ΔLIR^N) of ATG4B had a consistent, weak, but statistically insignificant, positive effect on GABARAPL1 cleavage while deletion of the C-terminal LIR (ΔLIR^C) strongly reduced cleavage of both LC3B and GABARAPL1 (Fig. 5E). When both LIRs were deleted there was a slight positive effect relative to deletion of the C-terminal LIR. This is consistent with the data of Satoo et al.,[37] showing that deletion of LIR^N resulted in more active cleavage in vitro. Taken together, our results support the conclusion that the C-terminal LIR is important for binding and required for effective cleavage of LC3B and GABARAPL1.

Next, we looked at subcellular distribution of endogenous LC3B in *atg4b* KO MEFs reconstituted with GFP, GFP-ATG4B WT, -C74S or -ΔLIR^C mutants. We observed a much higher number of LC3B dots in cells expressing catalytically active ATG4B constructs (WT and -ΔLIR^C) than in cells lacking ATG4B or expressing the C74S mutant (Fig. 6A and B). The presence of LC3B dots correlated with the detection of LC3B-II in western blot experiments (Fig. 5B), indicating autophagosome formation occurs in *atg4b* KO cells expressing active forms of ATG4B. There was no striking difference in the number of LC3B positive dots between cells expressing WT ATG4B or ATG4B ΔLIR^C (Fig. 6A). However, this number was consistently slightly higher in cells expressing the ATG4B ΔLIR^C construct than in cells expressing WT ATG4B (Fig. 6B).

To look at the importance of the LIR^C motif in ATG4B for autophagosome formation, cell lines stably expressing GFP-ATG4B WT or GFP-ATG4B ΔLIR^C were transiently transfected with mCherry-GFP-LC3B. Using this marker, autophagosomes emit green and red (yellow) fluorescence due to the recruitment of LC3B, while autolysosomes are only red because the green fluorescence is lost within acidic structures.[18] Expression of GFP-ATG4B in the stably expressing cell lines was not induced with doxycycline, therefore the fluorescent signals were only detected from the mCherry-GFP-LC3B construct. While cells expressing mCherry-GFP-LC3B but lacking ATG4B contained no yellow dots and few red only dots, cells expressing GFP-ATG4B WT or GFP-ATG4B ΔLIR^C contained many red only dots and also numerous yellow dots indicating autophagosome formation (Fig. 6C). Interestingly, cells expressing the ATG4B ΔLIR^C construct often contained mCherry-and GFP-positive ring structures larger than 1 μm. Such structures were rarely seen in cells expressing WT ATG4B (Fig. 6C). Given these results, we suggest that delipidation is impaired, resulting in a deregulated growth of phagophores and thereby a larger size of autophagosomes.

The LIR^C motif of ATG4B is required for stabilization of GABARAP and GABARAPL1 in vivo

Transient transfection of WT ATG4B has previously been shown to stabilize the unlipidated form of LC3B, and thereby inhibit the delivery of LC3B to ATG7.[36] We similarily observed that doxycycline-induced overexpression of WT ATG4B reduced lipidation of LC3B (Fig. 5B). However, when we compared uninduced cells with low expression of the various GFP-ATG4B constructs, there was no apparent sequestration of unlipidated LC3 or GABARAPL2 (Fig. 5B and Fig. 7A). The cellular pools of LC3B-I were basically similar in all the reconstituted cell lines, and affected neither by the presence or absence of ATG4B nor by the expression of a LIR^C mutated construct (Fig. 7A). The formation of LC3B-II clearly depends on the expression of catalytically active ATG4B, but unless highly overexpressed,[36] there was no apparent difference in LC3B-II formation between cell lines expressing WT or LIR^C mutated ATG4B constructs.

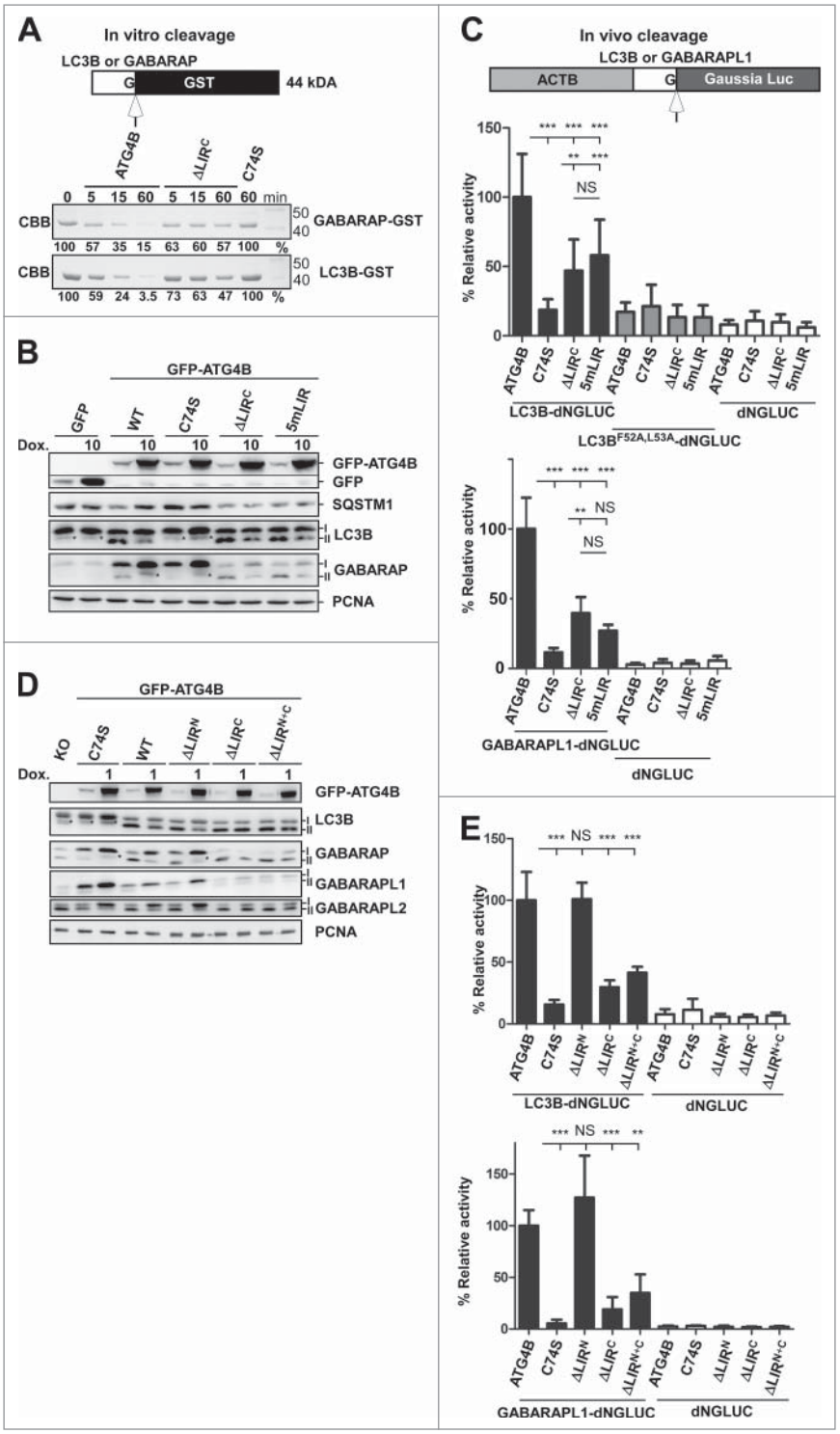

Figure 5. The C-terminal LIR motif of ATG4B is important for efficient cleavage of Atg8-family proteins. (A) GST-ATG4B ΔLIR^{C} displays reduced ability to cleave off a C-terminal GST tag on both LC3B and GABARAP. The GST-tagged substrates were incubated with recombinant ATG4B (WT or mutated) for 0, 5, 15 or 60 min. The rate of cleavage was measured after SDS-PAGE as a loss of the band corresponding to the GST-tagged substrate. The % of uncleaved substrate remaining is indicated. (B) Lipidation of LC3 and GABARAP is functional in *atg4b* knockout cells rescued with WT or LIR^{C} mutated GFP-ATG4B. Cells rescued with GFP-ATG4B constructs were treated or not with doxycycline (10 μg/ml) for 24 h to induce expression and cell lysates analyzed by western blotting. (C) Reduced ability of LIR^{C} mutated ATG4B constructs to cleave transiently transfected LC3B or GABARAPL1 fused to the Gaussia luciferase. Cells reconstituted with the indicated ATG4B constructs were transiently transfected with the indicated LC3B or GABARAPL1 Gaussia luciferase constructs or vector control. Cleavage was measured by release of Gaussia luciferase over a period of 18 to 24 h for cells expressing the indicated LC3B or GABARAPL1 Gaussia luciferase constructs or vector control. Mean +/− SD of 4 independent experiments, wild type set to 100%, n $\geq$ 6, NS P $>$ 0.05 $^{*}P \leq 0.05$, $^{**}P \leq 0.01$, $^{***}P \leq 0.001$. One-way ANNOVA followed by the Tukey multiple comparison test. (D) Deletion of LIR^{N} in ATG4B has no effect on lipidation of LC3B, GABARAP, GABARAPL1 or GABARAPL2 in *atg4b* knockout cells rescued with GFP-ATG4B. Cells rescued with WT or mutated GFP-ATG4B were treated or not with doxycycline (1 μg/ml) for 24 h to induce expression and cell lysates analyzed by western blotting. (E) Deletion of LIR^{N} has a slightly positive effect on cleavage of transiently transfected LC3B or GABARAPL1 fused to the Gaussia luciferase. Cells reconstituted with the indicated ATG4B constructs were transiently transfected with the indicated constructs and in vivo cleavage measured as in (C). Mean +/− SD of 3 independent experiments, wild type set to 100%, n $\geq$ 6, NS P $>$ 0.05 $^{*}P \leq 0.05$, $^{**}P \leq 0.01$, $^{***}P \leq 0.001$. One-way ANNOVA followed by the Tukey multiple comparison test.

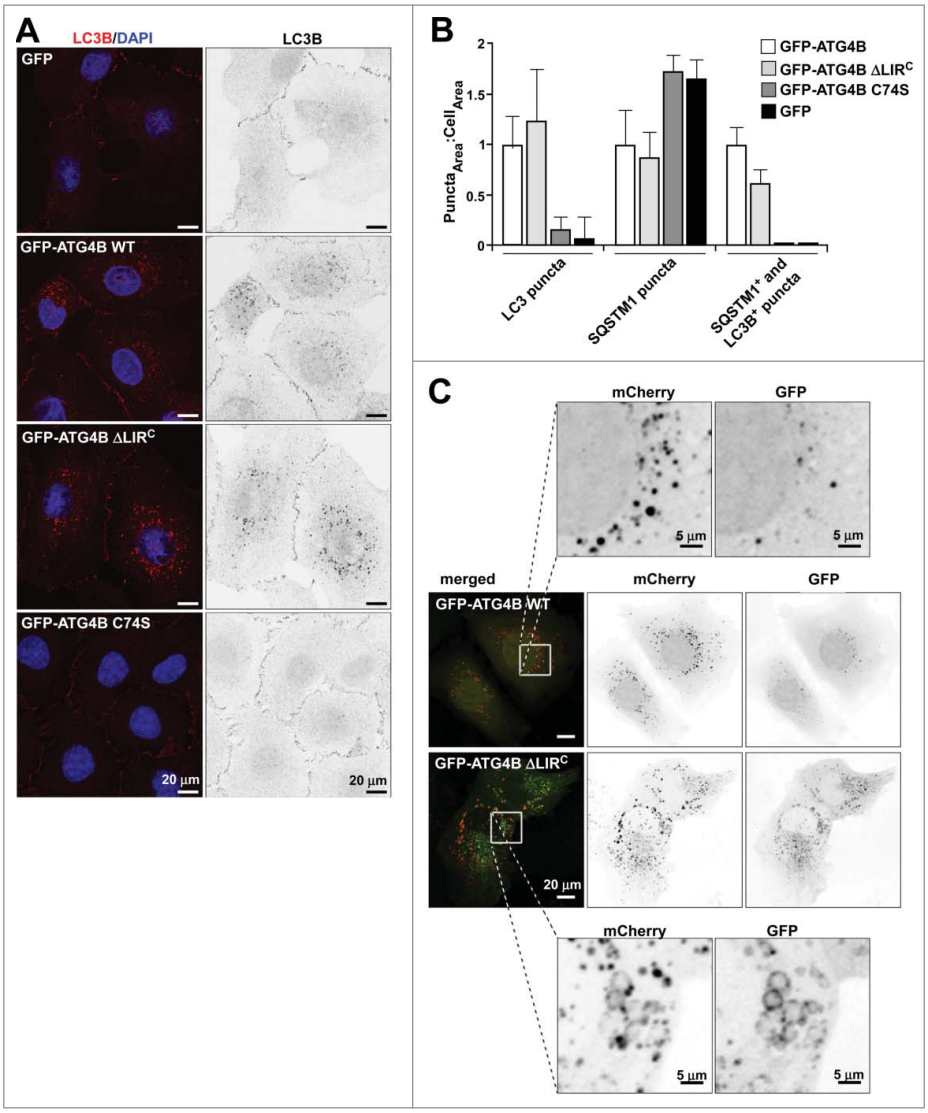

Figure 6. LC3B puncta formation is similar in *atg4b* KO MEFs expressing WT or LIR^C-deleted GFP-ATG4B. (A) Cells were stained with LC3B antibodies and analyzed by confocal imaging. (B) Quantification of fractions of cells containing LC3 puncta, SQSTM1 puncta, or puncta positive for both LC3B and SQSTM1. (C) *atg4b* KO MEFs reconstituted with WT or LIR^C-deleted GFP-ATG4B were transiently transfected with mCherry-GFP-LC3B, and analyzed by confocal imaging 16 h after transfection. There was no difference in yellow or red only structures between the cell lines, but cells expressing the LIR^C-deleted construct contained large ring structures rarely seen in cells expressing WT ATG4B. Note that cells were not treated with doxycycline, and expression of GFP-ATG4B was therefore below detection level in these studies.

In sharp contrast to LC3B and GABARAPL2, the cellular pools of unlipidated GABARAP and GABARAPL1 were strongly affected both by the presence of ATG4B and by a mutation of the LIR^C motif (Fig. 7A). As previously noted,[43] loss of ATG4B results in a severe reduction of unlipidated GABARAP and GABARAPL1 (Fig. 7A, lanes 1,2). A similar reduction in unlipidated LC3B was not seen in cells lacking ATG4B (Fig. 7A). Furthermore, while cells expressing WT or GFP-ATG4B (C74S) contained unlipidated GABARAP and GABARAPL1 (Fig. 7A, lanes 3,4), these pools of unlipidated GABARAP and GABARAPL1 were strongly reduced in cells expressing LIR^C mutated GFP-ATG4B constructs (Fig. 7A, lanes 5,6). Thus, ATG4B stabilizes GABARAP and GABARAPL1, and this stabilization is dependent on the C-terminal LIR motif. Mutation of the putative phosphorylated p-S392 residue,[41] to A or E, had no apparent effect on the stabilization or lipidation of Atg8-family orthologs (Fig. 7A, lanes 7 to 9), neither did the expression of a LIR^N deleted ATG4B (Fig. 5D). Surprisingly, elevated expression of ATG4A or ATG4C could not compensate for the lack of ATG4B (Fig. 7A, lanes 10 to 12). Treatment of *atg4b* KO cells with the proteasomal inhibitor MG132 resulted in accumulation of unlipidated GABARAP and GABARAPL1 (Fig. 7B, lanes 1,2 and 7,8), while inhibition of lysosomal degradation with bafilomycin A_1 (BafA1) only very weakly increased the level of GABARAP (Fig. 7C, lanes 2 and 7, and Fig. S6A). Hence, unlipidated GABARAP and GABARAPL1 are efficiently degraded by the proteasome in cells lacking ATG4B. In contrast, in cells expressing ATG4B WT, C74S or ΔLIR^C, both forms of GABARAP accumulated in BafA1-treated cells, and not in the MG132-treated cells (Fig. 7B, C). This suggests that ATG4B directs GABARAP to lysosomal degradation pathways.

To further demonstrate a correlation between the level of WT ATG4B and the levels of unlipidated and lipidated GABARAP, we analyzed cells expressing increasing amounts of ATG4B (Fig. 7D). We used cells treated or not with

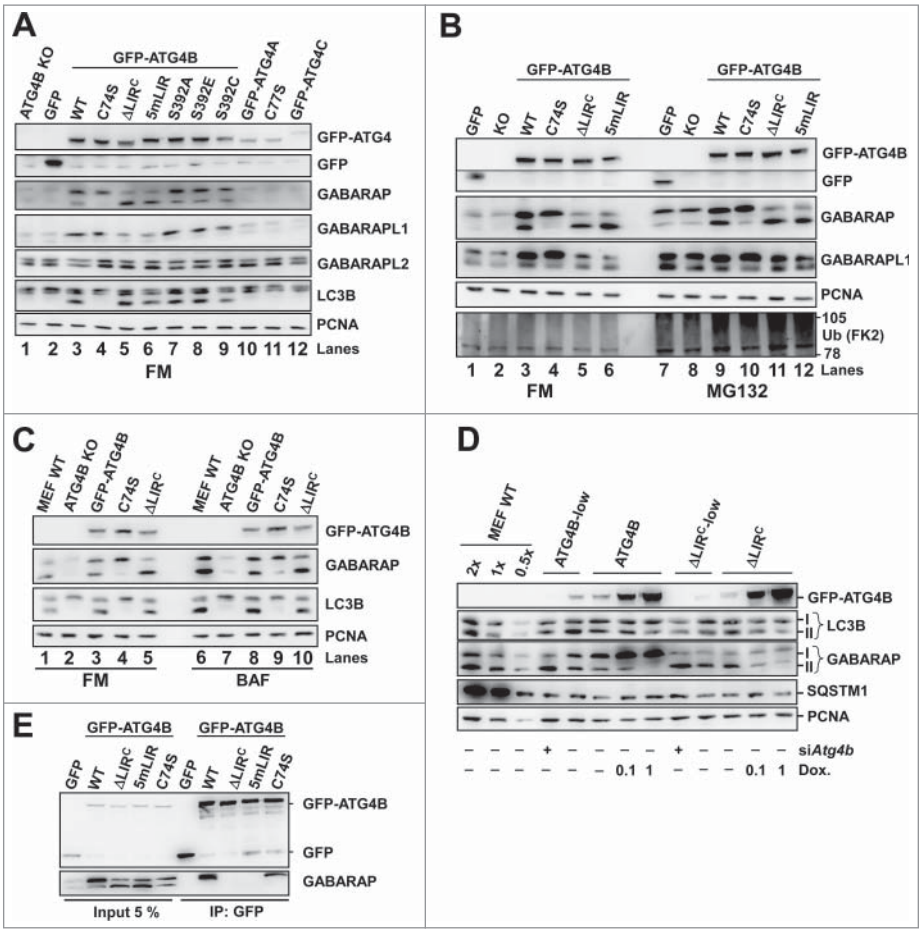

Figure 7. The LIR^C motif of ATG4B is required for stabilization of GABARAP and GABARAPL1. (A) The endogenous level of GABARAP is severely diminished in cells that do not express ATG4B. Extracts of *atg4b* KO cells reconstituted with the indicated GFP-ATG4 constructs were analyzed by western blotting. (B) GABARAP is degraded by the proteasome in cells that do not express ATG4B. Cells reconstituted with GFP or indicated GFP-ATG4B constructs were treated or not with the proteasomal inhibitor MG132 (10 μM) for 4 h and analyzed by western blotting. The FK2 anti-ubiquitin antibody was used as a positive control for proteasomal inhibition. (C) In cells that do not express ATG4B, or inactive ATG4B, there is very little, if any, accumulation of GABARAP in response to lysosomal inhibition by BafA1. Cells were treated with or without BafA1 (0.2 μM) for 8 h, and cell lysates analyzed by western blotting. (D) GABARAP, but not LC3B, is stabilized by an elevated expression of WT ATG4B, and stabilization is LIR^C dependent. Cell lysates from cells expressing different amounts of GFP-ATG4B or GFP-ATG4B ΔLIR^C were analyzed by western blotting. To increase or reduce the expression of GFP-ATG4B, cells were treated as indicated with doxycycline (0.1 or 1 μM) or *Atg4b* siRNA for 48 h, respectively. (E) Endogenous GABARAP is efficiently immunoprecipitated by ATG4B in a LIR^C-dependent manner. Lysates of *atg4b* KO cells reconstituted with the indicated GFP-ATG4B constructs were immunoprecipitated with GFP antibodies and analyzed by western blotting.

doxycycline. To increase the sensitivity of the assay we also used flow cytometry to select cells with lower expression of ATG4B than our initial clones (ATG4B-low and ΔLIR^C-low). In addition, these cells were transfected with siRNA against *Atg4b* to further reduce expression levels. The level of unlipidated GABARAP-I gradually increased when the level of WT ATG4B increased, reflecting stabilization of unlipidated GABARAP by ATG4B. No stabilization of GABARAP-I was seen in cells expressing increasing amounts of ATG4B ΔLIR^C (Fig. 7D). Thus, the ability of ATG4B to stabilize unlipidated GABARAP strongly depends on its LIR^C motif. In a similar type of experiment performed with cells expressing LIR^N-deleted constructs, it appeared that a deletion of LIR^N had no effect on the stabilization of GABARAP (Fig. S6B).

For cells expressing ATG4B WT, we observed a gradual decrease in the level of lipidated GABARAP (II form) correlating with the level of ATG4B (Fig. 7D). The high amount of GABARAP-II in cells expressing very little ATG4B indicates that the initial cleavage is efficient even with low ATG4B concentrations. Presumably, elevated ATG4B may reduce the amount of lipidated GABARAP both because it stabilizes the unlipidated form and because it increases delipidation from the phagophore. For cells expressing ATG4B ΔLIR^C, the II form was reduced in response to high overexpression, but the effect was weaker than seen for WT ATG4B (Fig. 7D).

The LIR^C dependent stabilization of GABARAP and GABARAPL1 by ATG4B indicates that these proteins form a stable complex in cells. To test this, GFP or GFP-tagged ATG4B proteins (WT or mutated) were immunoprecipitated from KO cells reconstituted with these constructs and coprecipitated endogenous GABARAP was detected by western blotting. Interestingly, GABARAP was efficiently coprecipitated with WT GFP-ATG4B and the catalytic inactive GFP-ATG4B (C74S), but not with the LIR^C mutated GFP-ATG4B proteins (Fig. 7E). This supports the conclusion that ATG4B forms a stable interaction with GABARAP that depends on the LIR^C motif. Without induction of GFP-ATG4B expression, no detectable coprecipitation of LC3B was seen. However, after induction of GFP-ATG4B expression with doxycycline, a weak and LIR^C dependent coprecipitation of endogenous LC3B was also seen (Fig. S6C). The

coprecipitation of LC3B was much less efficient than coprecipitation of GABARAP (Fig. S6C). The strongest LC3B interaction was consistently seen with the GFP-ATG4B (C74S) construct.

Next, the intracellular location of endogenous GABARAP in the *atg4b* KO MEFs reconstituted with different GFP-ATG4B constructs was studied by confocal imaging. In the cell lines reconstituted with catalytically active ATG4B GABARAP accumulated in dots dispersed throughout the cytoplasm, as well as in centrosomes identified as distinct TUBG/γ-tubulin positive dots (Fig. S7). The dots represent autophagic structures as some colocalize with LC3B and some with the early autophagosome marker WIPI2. This is in line with previous results suggesting a scaffolding role for GABARAP in autophagosome formation.[19,45] Surprisingly, in contrast to the western blot results (Fig. 5B), there was no significant increase in endogenous GABARAP staining in the cell lines reconstituted with WT or catalytic inactive ATG4B. We tested several antibodies with the same results. We therefore think that there is a problem with exposure of the epitope(s) recognized by the antibodies in the heterodimeric ATG4B-GABARAP complex. Consistent with the observed destabilization of endogenous GABARAP (Fig. 5B), ectopically expressed mCherry-GABARAP was not detected by confocal microscopy in *atg4b* KO cells. Reconstitution of the KO cells with low levels of WT GFP-ATG4B or GFP-ATG4B ΔLIR^{C} resulted in accumulation of mCherry-GABARAP dots similarly to the WT cells (Fig. 8A). Interestingly, induction of a high level WT GFP-ATG4B expression redistributed mCherry-GABARAP into a highly diffuse localization pattern (Fig. 8B), whereas high-level expression of GFP-ATG4B ΔLIR^{C} did not (Fig. 8B). Furthermore, cells reconstituted with the catalytically inactive C74S mutant redistributed mCherry-GABARAP into a diffuse localization pattern (Fig. 8A to C). Presumably, the dots represent phagophores and autophagosomes, while the diffuse mCherry-GABARAP constitutes the ATG4B associated pool of unlipidated GABARAP. Taken together, all our data clearly demonstrate a strong LIR^{C}-dependent interaction between ATG4B and GABARAP in cells. As depicted (Fig. 8D), a pool of unlipidated GABARAP may be stabilized by a LIR^{C}-dependent direct interaction between ATG4B and GABARAP. This may negatively regulate autophagosome formation by inhibiting the delivery of the cleaved product to ATG7, or may be required for the maintenance of an unlipidated pool of GABARAP that can be used upon autophagy induction.

Discussion

In this study, we identified a canonical LIR motif in the C terminus of ATG4B required for efficient binding of ATG4B to Atg8-family proteins, and for efficient cleavage of Atg8-family proteins both in vitro and in vivo. Previous structural studies of complexes formed between LC3B and ATG4B have been performed with C-terminally truncated ATG4B lacking the LIR^{C} motif because the high flexibility of the C-terminal residues (355 to 393) of human (*Homo sapiens*/Hs) ATG4 precluded crystallization.[37] The C-terminal LIR interaction was therefore not detected. Our results show that a strong interaction with LC3s and GABARAPs depends on simultaneous interactions with the catalytic domain and the LIR^{C} motif of ATG4B. Molecular modeling suggests that the linker between the catalytic domain and the LIR^{C} motif is long enough to adopt into a structure connecting the catalytic domain attached to LC3B with the LIR^{C} motif attached to LDS on the opposite side of LC3B. Since the LIR^{C} motif was equally important for binding as for cleavage, we have no evidence that the C terminus of ATG4B directly participates in the catalytic reaction. We therefore think that the increase in cleavage seen with LIR^{C}-containing constructs primarily is caused by a more efficient binding to Atg8-family proteins. In agreement with this view, the C-terminal region of *Xenopus laevis* ATG4B is reported to be important for in vitro cleavage of Atg8-family orthologs.[46]

LIR-LDS interaction may be regulated by phosphorylation.[13] A recent study reports that 2 sites in the C-terminal region of ATG4B (S383 and S392) are regulated in vivo by phosphorylation, and the phosphorylation of these sites increases after treatment of cells with the MTORC1 inhibitor rapamycin.[41] These sites flank the LIR^{C} motif. However, in our crystal structure, phosphorylated S392 pointed toward the solvent and the phosphomimetic mutation of these residues (S383E or S392E) did not significantly affect LIR^{C} binding. Further studies are needed to evaluate the regulatory importance of these sites in vivo.

The cleavage of proteins of the Atg8-family by ATG4B provides the primed conjugation-ready form (the I form) and is an essential step in phagophore formation. ATG4B also regulates the delipidation of Atg8-family proteins from the outer membrane of the phagophore.[16,32–34] A continuous lipidation and delipidation of Atg8-family proteins on the phagophore may act as a cyclical proofreading event to control the fidelity of growth of autophagosomes.[32] In yeast, Atg4 removes Atg8–PE from nonPAS organelle membranes. This may be critical for maintaining a pool of unlipidated Atg8 during autophagosome formation.[33,34] The lipidation and delipidation of yeast Atg8 has been reconstituted in vitro on giant unilamellar vesicles.[16] On these structures, Atg8–PE associated with Atg12–Atg5-Atg16 into a mesh-like membrane scaffold. Atg4 first disrupts the scaffold before delipidating Atg8. Our finding of a very efficient C-terminal LIR in ATG4B suggests that ATG4B may use the LIR^{C} to compete out GABARAP and LC3 interactions with ATG12–ATG5 and disrupt the membrane scaffold before delipidating. It is therefore tempting to speculate that the LIR^{C} motif is particularly important in the delipidation step, and even more so under endogenous conditions with limiting amounts of ATG4B. Delipidation occurs on membrane surfaces where Atg8-family molecules are enriched, and the process is therefore likely to involve both *cis* and *trans* type LIR-LDS interactions (Fig. 8D and E). The C-terminal LIR-LDS interaction may potentially act in *cis* or *trans*, but *trans*-interactions are most likely mediated by the N-terminal LIR motif which can only act in *trans*.[37] While the *cis*-interaction is necessary for the formation of a stable complex and for the maintenance of cellular pools of GABARAP and GABARAPL1, *trans*-interactions may be

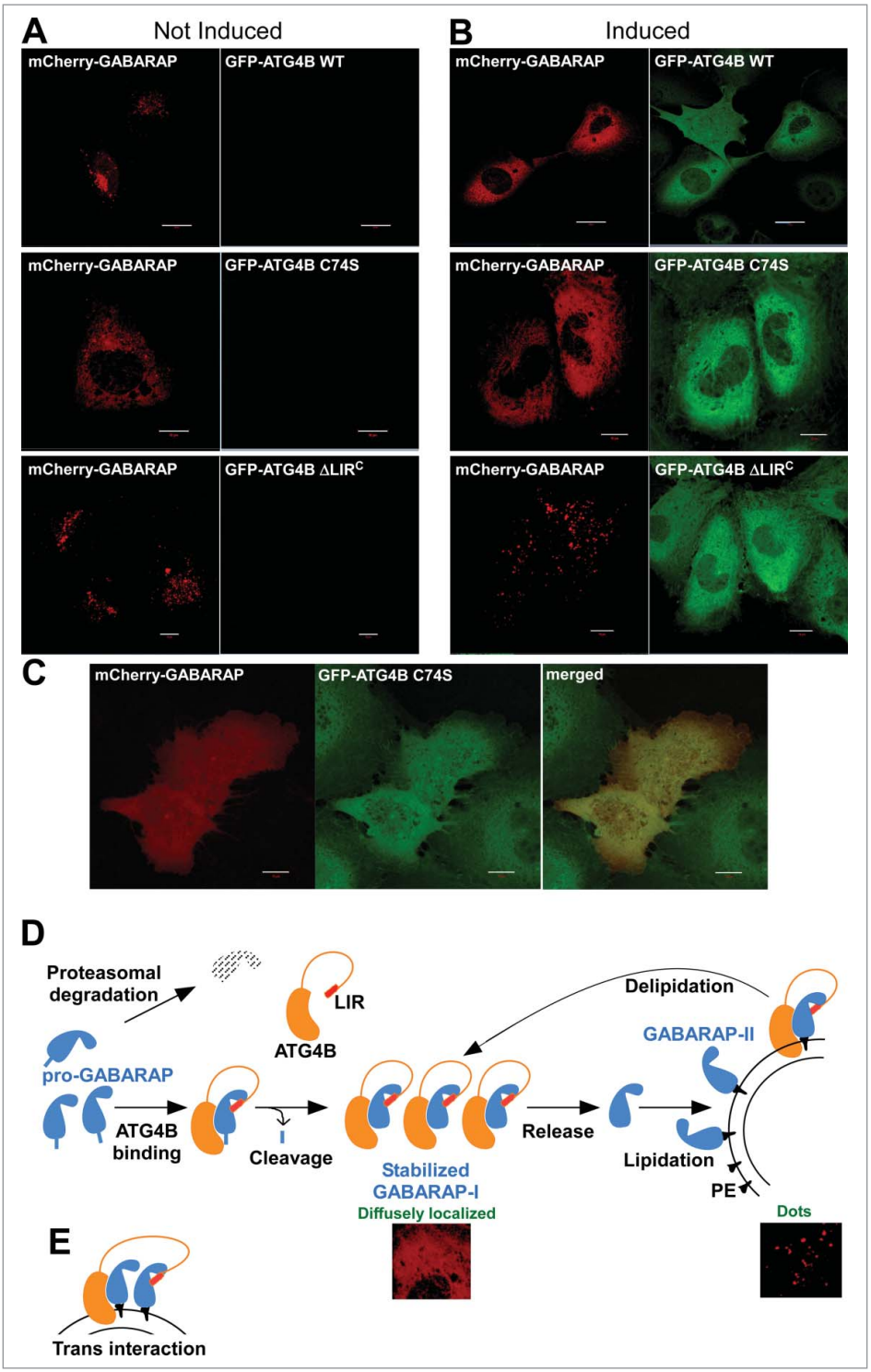

Figure 8. ATG4B stabilizes GABARAP in a LIR-dependent manner. (A) GABARAP stabilized by catalytic inactive ATG4B has a diffuse localization pattern in cells. *atg4b* KO cells reconstituted with GFP-ATG4B WT, C74S or ΔLIR^{C} mutant were transiently transfected with mCherry-GABARAP and analyzed by confocal microscopy 24 h post transfection. (B) High-level expression of ATG4B WT and catalytic inactive, but not ATG4B ΔLIR^{C}, stabilizes and redistributes ectopically expressed mCherry-GABARAP into a diffuse localization pattern. *atg4b* KO cells reconstituted with GFP-ATG4B WT, C74S or ΔLIR^{C} mutant were transiently transfected with mCherry-GABARAP, induced with doxycycline (1 μg/ml), and analyzed by confocal microscopy 24 h post transfection. (C) GFP-ATG4B (C74S) and ectopically expressed mCherry-GABARAP display an almost completely overlapping localization pattern, both in the cytoplasm and in the cell nucleus. *atg4b* KO cells reconstituted with GFP-ATG4B (C74S) were transiently transfected with mCherry-GABARAP, induced by doxycycline (1 μg/ml), and analyzed by confocal microscopy 24 h post transfection. Representative images are shown. Bars: 10 μm. (D) Illustration of functional activities of ATG4B, indicating how the C-terminal LIR stabilizes the interaction between ATG4B and GABARAP and thereby contributes to the maintenance of a pool of unlipidated GABARAP. In (E) a potential *trans*-mediated interaction of the C-terminal LIR with an adjacent Atg8-family molecule conjugated to the same membrane is illustrated.

more important during dynamic processes such as delipidation. Structural data show that is sterically possible that a single ATG4B molecule may be engaged in 3 interactions with 2 neighboring molecules of the Atg8 family. The substrate Atg8-family molecule is bound in *cis* by the C-terminal LIR and at the catalytic site, and the neighbor molecule

of the Atg8 family is bound in *trans* by the N-terminal LIR. This may facilitate efficient activation and delipidation on membrane surfaces.

The most dramatic effect seen in cells expressing a mutated LIR^C or a LIR^C-deleted GFP-ATG4B was a strong reduction in the cellular pools of unlipidated GABARAP and GABARAPL1, while the levels of LC3B and GABARAPL2 were unaffected. Previous studies have shown that the presence of unlipidated pools of Atg8-family proteins at least in part relies on their recycling from membranes by ATG4-dependent delipidation.[30–32] However, other studies have revealed that overexpressed ATG4B stabilizes unlipidated LC3B by preventing its delivery to ATG7.[36] Our study indicates that the formation of stable complexes between ATG4B and GABARAP or GABARAPL1 may be equally important as delipidation for the maintenance of unlipidated pools of these Atg8-family proteins.

Intriguingly, we observed that GABARAP and GABARAPL1 were degraded and virtually absent in cells lacking ATG4B. Consistently, the levels of these 2 proteins were highly elevated in cells overexpressing WT ATG4B. We propose that binding to ATG4B stabilizes these proteins. Without this stabilization they are rapidly degraded by the proteasome and unavailable for autophagosome formation. Hence, direct binding of ATG4B to GABARAP and GABARAPL1, depending on the C-terminal LIR motif, plays an important role in maintaining unlipidated pools of these 2 Atg8-family proteins. Potentially, the direct binding of ATG4B to proteins of the Atg8-family may also inhibit their delivery to ATG7 and thereby have a negative effect on autophagosome formation. Given that the presence of the LIR^C motif positively affects binding and cleavage of Atg8-family proteins, but negatively affects their release from ATG4B, the full complexity of these interactions are not easily reconstituted in a system based on ectopic overexpression of ATG4B mutants. Despite numerous attempts, we were unable to reconstitute *atg4b* KO MEFs at an endogenous expression level. In line with a previous report,[36] we show here that an elevated cellular pool of WT ATG4B has a negative effect on autophagosome formation: This is presumably because its inhibitory effect on the release of Atg8-family proteins then becomes dominant. However, at an endogenous expression level, the relative impact of binding and cleavage becomes crucial. Very likely, the LIR^C motif may then have a positive effect on autophagosome formation due to an increased rate of binding and cleavage of proteins of the Atg8 family.

Importantly, the C-terminal LIR motif in ATG4B increases the complexity of ATG4B interactions and thereby adds another layer of regulation of autophagosome biogenesis. This may have important regulatory consequences. In *C. elegans* GABARAP (LGG-1) acts upstream of LC3 (LGG-2) in removal of paternally inherited mitochondria in embryos,[47] and nonredundantly in autophagic degradation of PGL granules during embryogenesis.[48] LGG-1 and LGG-2 differentially interact with autophagy substrates and Atg proteins. Excess lipidated LGG-1 inhibited LGG-2 puncta formation, and UNC-51 (Atg1/ULK1 ortholog) interacted with LGG-1, but not LGG-2.[48] We have previously shown that the ULK complex members ULK1/2, RB1CC1, and ATG13 bind GABARAP preferentially via LIR motifs,[19] and that knockdown of GABARAP specifically attenuates ULK1 activation.[45] Hence, GABARAP may be involved in scaffolding this complex on autophagic structures. WAC (WW domain-containing adaptor with coiled-coil), a positive regulator of autophagy,[49] inhibits binding of GABARAP to the vesicle tethering GOLGA2/golgin A2/GM130 (golgi autoantigen, golgin subfamily a, 2) to release unlipidated GABARAP from the centrosome enabling its transport to autophagosome formation sites.[45] We show here that in addition to the centrosomal pool of GABARAP there is also a large pool of diffusely localized, unlipidated GABARAP bound to ATG4B. Further studies are needed to elucidate the regulatory roles of the ATG4B-GABARAP interaction, particularly during starvation and other stress conditions inducing autophagy.

Materials and methods

Plasmids

The Gateway entry clones used in this study were pENTR-ATG4A (Harvard PlasmID Repository, HsCD00372535), pENTR-ATG4B, pDONR-ATG4C (Harvard PlasmID Repository, HsCD00044545), pENTR-ATG4D (Harvard PlasmID Repository, HsCD00383159), pENTR-ATG4, pENTR-GABARAP, pENTR-GABARAPL1, pENTR-GABARAPL2, pENTR-LC3A, pENTR-LC3B, pENTR-LC3C, pENTR-Atg8. Point mutants of pENTR-ATG4A (1 to 389, C77S), pENTR-ATG4B [1 to 384, 12 to 393, 12 to 384, (Y8A and L11A), (F388A and L391A), (Y8A, L11A, F388A and L391A), C74S, (D385A, E386A, D387A, F388A and L391A), S383E, E386A, E389A, (E386A and E389A), S392A, S392E, (S392E and S383E), and S392C], pENTR-ATG4B 374 to 393 [(F388A and L391A), E384A, D385A, E386A, D387A, E389A, S383A, S383E, S392A and S392E], pENTR-ATG4C (1 to 451), pENTR-ATG4D (1 to 467), pENTR-ATG4 [1 to 340, (F343A and L346A), (Y424A and I427A), (F446A and I449A)], pENTR-LC3B [(R10A and R11A), (F52A and L53A), R70A and (F80A and L82A)], pENTR-GABARAPL1 [H9A, R28A, R47A, (H9A and R47A), Y49A and R67A], and pENTR-Atg8 (Y49A) were made using the QuikChange site-directed mutagenesis kit (Agilent Technologies, 210515). pENTR-ATG4B were made by subcloning of ATG4B into pENTR1A (Thermo Fisher Scientific, A10462) from pOTB7-ATG4B (Harvard PlasmID Repository, HsCD00324503). Generation of constructs containing the C-terminal region of ATG4B (374 to 393 or 365 to 384) were made by subcloning into pENTR1A. ACTB-LC3B (F52A,L53A)-dNGLUC and ACTB-GABARAPL1-dNGLUC were established by mutagenesis and subcloning into the ACTB-LC3-dNGLUC plasmid (kind gifts from Robin Ketteler and Bryan Seed, Medical Research Council, Laboratory for Molecular and Cell Biology, University College London). The plasmid for recombinant expression of yeast Atg4 fused to GST was a kind gift of Sascha Martens (Department of Biochemistry and Cell Biology, Max F. Perutz Laboratories, University of Vienna). Yeast Atg4 was inserted into pENTR1A by subcloning. Gateway destination vectors used were pDEST15 (bacterial expression of N-terminal GST fusion proteins; Thermo Fisher Scientific, 11802014), pDEST24 (bacterial expression of C-terminal GST fusion proteins) (Thermo Fisher Scientific, 12216016), pDESTmyc (mammalian expression of N-terminal MYC-tagged proteins), pDEST-EGFP (mammalian expression of N-terminal EGFP-tagged proteins), and pDEST53 (mammalian expression of N-terminal GFP-tagged proteins; Thermo Fisher Scientific, 12288015). pDEST-LTR-EGFP (mammalian transfection vector for stable

and doxycycline controlled inducible expression of N-terminal-EGFP tagged fusion constructs under the control of a truncated *CMV* promoter) conferring blasticidin resistance was made by subcloning of EGFP and the GATEWAY cassette as a PCR product from pDEST-EGFP-C1 into the reverse Tetracycline retrovirus vector pLRT-X (a kind gift from Dr. Masaaki Komatsu, School of Medicine, Niigata University, Japan). Transfer of pENTR constructs to destination vectors was performed using the Gateway LR reaction (Thermo Fisher Scientific, 11791020).

Cell culture

MEFs were cultured in DMEM (Sigma-Aldrich, D6046) supplemented with 10% fetal bovine serum (Biochrom, S 0615) and 1% streptomycin-penicillin (Sigma-Aldrich, P4333). Knockdown of ATG4B was achieved by transfection of *Atg4b* siRNA (GAUUGGAGGUGGACACAAA, 50 nM) with Lipofectamine® RNAiMAX (Thermo Fisher Scientific, 13778030).

Generation of stable cell lines

ATG4B wild-type and knockout MEFs were obtained from Dr. Carlos Lòpez-Otín.[43] Cell lines stably expressing different GFP-ATG4 variants and GFP were made by transfection of Platinum Retroviral Packaging Cell Line-E (Cell Biolabs, RV-101) with pDEST-LTR plasmids containing the different GFP-ATG4 constructs or GFP. Viral supernatant was harvested, filtered through a 0.45-μM filter, supplemented with 8 μg/ml of polybrene (Sigma-Aldrich, H9268) and added to the *atg4b* knockout MEFs 24, 48 and 72 h post transfection. Immediately after viral transfection the MEFs were split and reseeded in medium containing 5 μg/ml blasticidin S HCl (Thermo Fisher Scientific, R210–01). Induction of GFP-tagged proteins was achieved by treatment of the stable cell lines with the indicated amounts of Doxycycline (Sigma-Aldrich, D9891) for 24 h unless otherwise stated.

Peptide arrays

Peptides were synthesized on cellulose membranes using a MultiPep automated peptide synthesizer (INTAVIS Bioanalytical Instruments AG, Cologne, Germany), as described previously.[50] Membranes were blocked using 5% nonfat dry milk in Tris-buffered saline (10 mM Tris-HCl, pH 7.4, 150 mM NaCl) containing 0.1% Tween 20 (Sigma-Aldrich, P1379). The membrane was probed by overlaying with 1 μg/ml of either GST, GST-LC3B or GST-GABARAPL1 for 2 h at RT. Membranes were washed 3 times in Tris-buffered saline containing 0.1% Tween 20. Bound protein were detected with HRP-conjugated anti-GST antibody (GE Healthcare, RPN1236)

Antibodies and reagents

The following antibodies were used: Rabbit anti-LC3B (Sigma-Aldrich, L7543), mouse anti-GABARAP (MBL, M135–3), rabbit anti-GABARAPL1 (Proteintech Group, 18723–1-AP), rabbit anti-GABARAPL2 (MBL, PM038) guinea pig anti-SQSTM1 (Progen, GP62-C), rabbit anti-GFP (Abcam, AB290), mouse anti-PCNA (DAKO, M0829), rabbit anti-ATG4B (Santa Cruz Biotechnology, SC-130968), mouse anti-ubiquitin (FK2; Enzo Life Sciences, PW8810), horseradish peroxidase-conjugated goat anti-mouse (BD Biosciences, 554002), anti-rabbit (BD Biosciences, 554021) and goat anti-guinea pig (Santa Cruz Biotechnology, sc-2438) secondary antibodies. Other reagents used were BafA1 (Santa Cruz Biotechnology, sc-201550) and l-[^{35}S] methionine (PerkinElmer, NEG709A500UC).

Protein purification and GST affinity isolation experiments

GST-tagged proteins were expressed in *Escherichia coli* BL21 (DE3). GST-(Atg8-family proteins) and (Atg8-family proteins)-GST fusion proteins were purified on glutathione-Sepharose 4 Fast Flow beads (GE Healthcare, 17513201) followed by washing with NET-N buffer (100 mM NaCl, 1 mM EDTA, 0.5% Nonidet P-40 (Sigma-Aldrich, 74385), 50 mM Tris-HCl, pH 8) supplemented with cOmplete Mini EDTA-free protease inhibitor mixture tablets (Roche Applied Science, 11836170001). GST-ATG4Bs fusion proteins were purified on GSTrap Fast Flow columns (GE Healthcare, 17–5130–01). GST-tagged proteins were eluated with 50 mM Tris, pH 8, 200 mM NaCl, 5 mM L-gluthathione reduced (Sigma-Aldrich, G425). GST affinity isolation assays were performed with ^{35}S-labeled proteins cotranscribed and translated using the TnT Coupled Reticulocyte Lysate System (Promega, L4610) as described previously.[18] For quantifications gels were vacuum dried and ^{35}S-labeled proteins detected on a Fujifilm bioimaging analyzer BAS-5000 (Fujifilm, Tokyo, Japan).

Expression and purification of GABARAPL1 for crystallization

GABARAPL1 full-length sequence was inserted between the BamHI and NotI sites of a pGEX-6P2 plasmid (GE Healthcare, 28–9546–50) containing a cleavable glutathione S-transferase tag. Protein expression was at 30°C in *E. coli* Rosetta (DE3) pLysS. Bacteria were harvested by centrifugation and resuspended in lysis buffer (50 mM Tris-HCl, pH 8.0, 500 mM NaCl, 0.1% Triton X-100 (Sigma-Aldrich, T8787), 0.5 mM TCEP (Melford Laboratories, T2650), 0.5 mM AEBSF (AppliChem, A1421) and 15 ug/ml benzamidine (Melford Laboratories, B4101). The fusion protein was batch-adsorbed onto a glutathione-Sepharose affinity matrix and GABARAPL1 recovered by cleavage with 3C protease (made in house) at 4°C overnight in 50 mM Tris-HCl, pH 8.0, 100 mM NaCl, 0.5 mM TCEP. GABARAPL1 was then purified by size exclusion chromatography using a Superdex 75 column equilibrated and run in 25 mM Tris-HCl, pH 8.0, 150 mM NaCl and 0.5 mM TCEP. Peptides were synthesized by the Francis Crick Institute Peptide Chemistry Science Technology Platform.

Crystallization of ATG4B LIR

GABARAPL1-ATG4B LIR complexes were prepared by mixing purified full-length GABARAPL1 and ATG4B peptide (residues 384 to 393, defined hereafter as wild-type ATG4B LIR; EDEDFEILSL) at a 1:3 molar ratio. The complex of the ATG4B peptide phosphorylated on residue S392 (residues 384 to 393, defined hereafter as phosphorylated ATG4B LIR;

EDEDFEIL-pS-L) was prepared by mixing GABARAPL1 and the phosphorylated ATG4B peptide at a 1:3 molar ratio. The complexes were dialyzed overnight in 25 mM Tris-HCl, pH 8.0, 150 mM NaCl and 0.5 mM TCEP buffer, using a 500- to 1000-Da MWCO dialysis tubing for both complexes. The wild-type ATG4B complex was crystallized at 20°C using the sitting-drop vapor diffusion method with a protein concentration of 20 mg/ml. Sitting drops of 1 μl consisted of a 1:1 (vol:vol) mixture of protein and a well solution containing 0.17 M $(NH_4)_2SO4$ (Hampton Research, HR2–541), 40% PEG 4000 (Sigma-Aldrich, 95904), 15% glycerol (Sigma-Aldrich, G5516). Crystals appeared after 10 d and reached their maximum size after 20 d (0.05 mm × 0.05 mm). Crystals were flash-frozen in liquid nitrogen, and X-ray data sets were collected at 100 K at the I02 beamline of the Diamond Light Source Synchrotron (Oxford, UK).

The phosphorylated ATG4B complex was crystallized at 20°C using the sitting-drop vapor diffusion method with a protein concentration of 20 mg/ml. Sitting drops of 1 μl consisted of a 1:1 (vol:vol) mixture of protein and a well solution containing 0.1 M $MgCl_2$, 24.6% PEG 400, 29.5% PEG 8000 (Sigma-Aldrich, 89510), 0.1M Tris, pH 8.5. Crystals appeared after 5 d and reached their maximum size after 10 d (0.2 mm × 0.05 mm). Crystals were flash-frozen in liquid nitrogen, and X-ray data sets were collected at 100 K at the I03 beamline of the Diamond Light Source Synchrotron (Oxford, UK).

Data collection and refinement statistics are summarized in Table 1. The data sets were indexed and scaled with xia2.[51] Molecular replacement was achieved by using the atomic coordinates of the peptide-free GABARAPL1 (PDB code: 2R2Q) in PHASER.[52] Refinement was performed using Phenix.[53] Model building was performed in COOT.[54] Model validation used PROCHECK,[55] and figures were prepared using the graphics program PYMOL (http://www.pymol.org). The asymmetric units contain 3 identical copies of the complex for the wild-type ATG4B-GABARAPL1 structure and 2 identical copies of the complex for the phosphorylated ATG4B-GABARAPL1 structure. In both structures the difference electron density map covering ATG4B shows unambiguous density for residues 484 to 493.

Table 1. Data collection and refinement statistics.

PDB ID	WT ATG4B-GABARAPL1 5LXH	ATG4B (p-S392)-GABARAPL1 5LXI
Data collection		
Space group	P 2_1 2_1 2_1	C 2
Cell dimensions a, b, c (Å) α, β, γ (°)	51.5, 79.89, 97.64 90.0, 90.0, 90.0	124.9, 78.4, 30.6 90.0, 99.2, 90.0
Resolution (Å) (Outer resolution shell) Å	51 – 1.58 (1.66 –1.58)	35 – 1.44 (1.48 –1.44)
Rpim	3.0 (49.4)	2.9 (50.9)
R_{sym} (%)	5.6 (87.9)	3.8 (59.0)
CC(1/2)	99.9 (60.5)	99.8 (74.6)
I/σI	10.7 (1.3)	10.1 (1.3)
Completeness (%)	100 (99.9)	96.0 (93.7)
Redundancy	5.1 (4.9)	3.1 (3.0)
Refinement		
Resolution (Å) (Outer resolution shell) Å	48 – 1.58 (1.60 – 1.58)	31 – 1.44 (1.47 – 1.44)
No. unique reflections	55 946	46 217
R_{work}	20.5 (39.1)	19.6 (36.3)
R_{free}[a]	23.7 (45.6)	22.9 (41.7)
No. atoms	3 467	2 290
Average isotropic *B*-factors (Å^2)	25.8	30.7
GABARAPL1	24.3	30.1
ATG4B peptide	43.6	35.0
Water	34.7	34.6
R.m.s. deviations		
bonds (Å)	0.017	0.014
angles (°)	1.42	1.15
Ramachandran plot (%) (favored, allowed, disallowed)	98.9/1.1/0	97.3/2.7/0

[a] A total of 5% of the data were set aside to compute R_{free}.

In vitro assay of ATG4B cleavage activity

LC3B-GST- and GABARAP-GST proteins expressed and purified from E. coli were washed 5 times to remove excess protease inhibitor. 2.5 μg/ml of GST-ATG4B, GST-ATG4B (C74S), or GST-ATG4B ΔLIR^C proteins were incubated together with 0.5 to 1.5 μg of LC3B-GST or GABARAP-GST at 30°C for the indicated time points in 20 μl buffer (200 mM NaCl, 1 mM EDTA, 5 mM DTT, 20 mM Tris-HCl, pH 7.4). Reactions were stopped by addition of 5xSDS-loading buffer (500 mM DTT, 10% SDS, 0.5% bromophenol blue, 50% glycerol, 250 mM Tris-HCl, pH 6.8), resolved by SDS-PAGE and visualized by Coomassie brilliant blue staining.

Western blot and immunoprecipitation experiments

For western blotting experiments, cells were washed in PBS (137 mM NaCl, 2.7 mM KCl, 4.3 mM Na_2HPO_4, 1.47 mM KH_2PO_4, pH 7.4.) followed by lysis directly in SDS-PAGE loading buffer (2% SDS, 10% glycerol 50 mM Tris-HCl, pH 6.8) and boiled for 10 min. Protein concentration was measured followed by addition of bromophenol blue (0.1%) and DTT (100 mM). Samples (20 μg) were run on 10–16% gradient- or 10%-SDS-polyacrylamide gels and blotted on Hybond nitrocellulose membranes (GE Healthcare, 10600003) followed by Ponceau S staining. Blocking was performed in 5% nonfat dry milk in PBS-Tween 20 (0.1%). Primary antibody was diluted in PBS-Tween 20 containing 5% nonfat dry milk and incubation was performed overnight at 4°C. Secondary antibody incubation was performed at room temperature for 1 h in PBS-Tween 20 containing 5% nonfat dry milk. Membranes were washes 3 times before addition of secondary antibody and development using either Amersham Hyperfilm ECL (GE Healthcare, 28906836) or LAS-300 (Fujifilm, Tokyo, Japan). Immunoprecipitations were performed by use of GFP-trap_A system in accordance with the manufacturer's instructions (Chromotek, gta-20).

Luciferase assay to monitor in vivo cleavage activity of ATG4B

In vivo ATG4B activity was assayed by measuring cellular export of Gaussia luciferase as described previously.[44] Reconstituted *atg4b* KO MEFs were seeded in 24-well plates and cotransfected with 50 ng pGL3 promotor (Firefly luciferase) (Promega, E1761) and 200 ng of either ACTB-LC3B-dNGLUC/ACTB-LC3B F52A L53A-dNGLUC/ACTB-GABARAPL1-dNGLUC or ACTB-dNGLUC using Metafectene Pro

(Biontex, T040). Media was changed 24 h post-transfection, and Gaussia luciferase was allowed to accumulate in the media for 18 to 24 h. Media and cells were harvested for measurements of Gaussia and Firefly luciferase, respectively, using the Dual luciferase reporter assay system (Promega, E1910) and a CLARIOstar (BMG labtech, Ortenberg, Germany) in accordance with the manufacturer's instructions. For ACTB-dNGLUC and ACTB-LC3B (F52A,L53A)-dNGLUC, single sampling tests were conducted on the cell lysate to verify that functional Gaussia luciferase was retained inside the cells.

Bioinformatics and statistics

Data in all figures are shown as mean ± SD from at least 3 independent experiments. Statistical significance was evaluated with one-way ANOVA followed by the Tukey multiple comparison test performed in PRISM (Graphpad) (ns $P > 0.05$, $^{*}P \leq 0.05$, $^{**}P \leq 0.01$, $^{***}P \leq 0.001$). Alignment of ATG4 isoform homologs was performed in CLC Main workbench (Qiagen).

Abbreviations

2mLIR, F388A and L391A	double mutation of LIR
5mLIR, D385A, E386A, D387A, F388A and L391A	multiple mutation of LIR
ATG	AuTophaGy-related
BafA1	Bafilomycin A_1
GABARAP	gamma-aminobutyric acid receptor associated protein
GFP	enhanced green fluorescent protein
KO	knockout
LDS	LIR docking site
LIR	LC3-interacting region
MAP1LC3/LC3	microtubule-associated protein 1 light chain 3
MEF	mouse embryonic fibroblast
PE	phosphatidylethanolamine

Disclosure of potential conflicts of interest

No potential conflicts of interest were disclosed.

Acknowledgments

We are indebted to Carlos Lòpez-Otín for the generous gift of the *atg4b* KO MEFs, to Robin Ketteler and Bryan Seed for the ACTB-LC3-dNGLUC and ACTB-dNGLUC plasmids, Dr. Masaaki Komatsu for the pLRT-X retovirus vector, and to Sascha Martens for the yeast GST-Atg4 plasmid. The technical assistance of Gry Evjen and Roy André Lysø is greatly appreciated. We thank the Advanced Microscopy Core Facility (AMCF) at the Institute of Medical Biology (UiT – The Arctic University of Norway) for the use of instrumentation and expert assistance. We thank the Francis Crick Institute Structural Biology Science Technology Platform for technical support.

Funding

This work was funded by grants from the FRIBIOMED program of the Norwegian Research Council (grant number 214448), and the Norwegian Cancer Society (grant number 71043-PR-2006–0320) to T.J., S.M., N. O'R., M.W. and S.A.T. were supported by the Francis Crick Institute (FC001187; M.W. and S.A.T.) which receives its core funding from Cancer Research UK, the UK Medical Research Council, and the Wellcome Trust.

ORCID

Sharon A. Tooze http://orcid.org/0000-0002-2182-3116
Terje Johansen http://orcid.org/0000-0003-1451-9578

References

[1] Mizushima N, Komatsu M. Autophagy: renovation of cells and tissues. Cell 2011; 147:728-41; PMID:22078875; http://dx.doi.org/10.1016/j.cell.2011.10.026
[2] Seglen PO. Regulation of autophagic protein degradation in isolated liver cells. In: Glaumann H, Ballard FJ, ed. Lysosomes: Their Role in Protein Breakdown. London: Academic Press, 1987:371-414
[3] Wen X, Klionsky DJ. An overview of macroautophagy in yeast. J Mol Biol 2016; 428:1681-99; PMID:26908221; http://dx.doi.org/10.1016/j.jmb.2016.02.021
[4] Johansen T, Lamark T. Selective autophagy mediated by autophagic adapter proteins. Autophagy 2011; 7:279-96; PMID:21189453; http://dx.doi.org/10.4161/auto.7.3.14487
[5] Rogov V, Dotsch V, Johansen T, Kirkin V. Interactions between autophagy receptors and ubiquitin-like proteins form the molecular basis for selective autophagy. Mol Cell 2014; 53:167-78; PMID:24462201; http://dx.doi.org/10.1016/j.molcel.2013.12.014
[6] Gordon PB, Seglen PO. Prelysosomal convergence of autophagic and endocytic pathways. Biochem Biophys Res Commun 1988; 151:40-7; PMID:3126737; http://dx.doi.org/10.1016/0006-291X(88)90556-6
[7] Shen HM, Mizushima N. At the end of the autophagic road: an emerging understanding of lysosomal functions in autophagy. Trends Biochem Sci 2014; 39:61-71; PMID:24369758; http://dx.doi.org/10.1016/j.tibs.2013.12.001
[8] Tsukada M, Ohsumi Y. Isolation and characterization of autophagy-defective mutants of Saccharomyces cerevisiae. FEBS Lett 1993; 333:169-74; PMID:8224160; http://dx.doi.org/10.1016/0014-5793(93)80398-E
[9] Mizushima N, Yoshimori T, Ohsumi Y. The role of Atg proteins in autophagosome formation. Annu Rev Cell Dev Biol 2011; 27:107-32; PMID:21801009; http://dx.doi.org/10.1146/annurev-cellbio-092910-154005
[10] Shpilka T, Weidberg H, Pietrokovski S, Elazar Z. Atg8: an autophagy-related ubiquitin-like protein family. Genome Biol 2011; 12:226; PMID:21867568; http://dx.doi.org/10.1186/gb-2011-12-7-226
[11] Ichimura Y, Kirisako T, Takao T, Satomi Y, Shimonishi Y, Ishihara N, Mizushima N, Tanida I, Kominami E, Ohsumi M, et al. A ubiquitin-like system mediates protein lipidation. Nature 2000; 408:488-92; PMID:11100732; http://dx.doi.org/10.1038/35044114
[12] Kabeya Y, Mizushima N, Ueno T, Yamamoto A, Kirisako T, Noda T, Kominami E, Ohsumi Y, Yoshimori T. LC3, a mammalian homologue of yeast Apg8p, is localized in autophagosome membranes after processing. EMBO J 2000; 19:5720-8; PMID:11060023; http://dx.doi.org/10.1093/emboj/19.21.5720
[13] Birgisdottir AB, Lamark T, Johansen T. The LIR motif - crucial for selective autophagy. J Cell Sci 2013; 126:3237-47; PMID:23908376
[14] Xie Z, Nair U, Klionsky DJ. Atg8 controls phagophore expansion during autophagosome formation. Mol Biol Cell 2008; 19:3290-8; PMID:18508918; http://dx.doi.org/10.1091/mbc.E07-12-1292
[15] Weidberg H, Shvets E, Shpilka T, Shimron F, Shinder V, Elazar Z. LC3 and GATE-16/GABARAP subfamilies are both essential yet act differently in autophagosome biogenesis. EMBO J 2010; 29:1792-802; PMID:20418806; http://dx.doi.org/10.1038/emboj.2010.74
[16] Kaufmann A, Beier V, Franquelim HG, Wollert T. Molecular mechanism of autophagic membrane-scaffold assembly and disassembly. Cell 2014; 156:469-81; PMID:24485455; http://dx.doi.org/10.1016/j.cell.2013.12.022
[17] Kirisako T, Ichimura Y, Okada H, Kabeya Y, Mizushima N, Yoshimori T, Ohsumi M, Takao T, Noda T, Ohsumi Y. The reversible modification regulates the membrane-binding state of Apg8/Aut7

essential for autophagy and the cytoplasm to vacuole targeting pathway. J Cell Biol 2000; 151:263-76; PMID:11038174; http://dx.doi.org/10.1083/jcb.151.2.263

[18] Pankiv S, Clausen TH, Lamark T, Brech A, Bruun JA, Outzen H, Overvatn A, Bjorkoy G, Johansen T. p62/SQSTM1 binds directly to Atg8/LC3 to facilitate degradation of ubiquitinated protein aggregates by autophagy. J Biol Chem 2007; 282:24131-45; PMID:17580304; http://dx.doi.org/10.1074/jbc.M702824200

[19] Alemu EA, Lamark T, Torgersen KM, Birgisdottir AB, Larsen KB, Jain A, Olsvik H, Overvatn A, Kirkin V, Johansen T. ATG8 family proteins act as scaffolds for assembly of the ULK complex: Sequence Requirements For LC3-Interacting Region (LIR) Motifs. J Biol Chem 2012; 287:39275-90; PMID:23043107; http://dx.doi.org/10.1074/jbc.M112.378109

[20] Hamacher-Brady A, Brady NR. Mitophagy programs: mechanisms and physiological implications of mitochondrial targeting by autophagy. Cell Mol Life Sci 2016; 73:775-95; PMID:26611876; http://dx.doi.org/10.1007/s00018-015-2087-8

[21] Wild P, McEwan DG, Dikic I. The LC3 interactome at a glance. J Cell Sci 2014; 127:3-9; PMID:24345374; http://dx.doi.org/10.1242/jcs.140426

[22] Ichimura Y, Kumanomidou T, Sou YS, Mizushima T, Ezaki J, Ueno T, Kominami E, Yamane T, Tanaka K, Komatsu M. Structural basis for sorting mechanism of p62 in selective autophagy. J Biol Chem 2008; 283:22847-57; PMID:18524774; http://dx.doi.org/10.1074/jbc.M802182200

[23] Noda NN, Kumeta H, Nakatogawa H, Satoo K, Adachi W, Ishii J, Fujioka Y, Ohsumi Y, Inagaki F. Structural basis of target recognition by Atg8/LC3 during selective autophagy. Genes Cells 2008; 13:1211-8; PMID:19021777; http://dx.doi.org/10.1111/j.1365-2443.2008.01238.x

[24] Fernandez AF, Lopez-Otin C. The functional and pathologic relevance of autophagy proteases. J Clin Invest 2015; 125:33-41; PMID:25654548; http://dx.doi.org/10.1172/JCI73940

[25] Hemelaar J, Lelyveld VS, Kessler BM, Ploegh HL. A single protease, Apg4B, is specific for the autophagy-related ubiquitin-like proteins GATE-16, MAP1-LC3, GABARAP, and Apg8L. J Biol Chem 2003; 278:51841-50; PMID:14530254; http://dx.doi.org/10.1074/jbc.M308762200

[26] Li M, Hou Y, Wang J, Chen X, Shao ZM, Yin XM. Kinetics comparisons of mammalian Atg4 homologues indicate selective preferences toward diverse Atg8 substrates. J Biol Chem 2011; 286:7327-38; PMID:21177865; http://dx.doi.org/10.1074/jbc.M110.199059

[27] Tanida I, Ueno T, Kominami E. Human light chain 3/MAP1LC3B is cleaved at its carboxyl-terminal Met121 to expose Gly120 for lipidation and targeting to autophagosomal membranes. J Biol Chem 2004; 279:47704-10; PMID:15355958; http://dx.doi.org/10.1074/jbc.M407016200

[28] Kabeya Y, Mizushima N, Yamamoto A, Oshitani-Okamoto S, Ohsumi Y, Yoshimori T. LC3, GABARAP and GATE16 localize to autophagosomal membrane depending on form-II formation. J Cell Sci 2004; 117:2805-12; PMID:15169837; http://dx.doi.org/10.1242/jcs.01131

[29] Scherz-Shouval R, Sagiv Y, Shorer H, Elazar Z. The COOH terminus of GATE-16, an intra-Golgi transport modulator, is cleaved by the human cysteine protease HsApg4A. J Biol Chem 2003; 278:14053-8; PMID:12473658; http://dx.doi.org/10.1074/jbc.M212108200

[30] Betin VM, Lane JD. Caspase cleavage of Atg4D stimulates GABARAP-L1 processing and triggers mitochondrial targeting and apoptosis. J Cell Sci 2009; 122:2554-66; PMID:19549685; http://dx.doi.org/10.1242/jcs.046250

[31] Marino G, Salvador-Montoliu N, Fueyo A, Knecht E, Mizushima N, Lopez-Otin C. Tissue-specific autophagy alterations and increased tumorigenesis in mice deficient in Atg4C/autophagin-3. J Biol Chem 2007; 282:18573-83; PMID:17442669; http://dx.doi.org/10.1074/jbc.M701194200

[32] Nair U, Yen WL, Mari M, Cao Y, Xie Z, Baba M, Reggiori F, Klionsky DJ. A role for Atg8-PE deconjugation in autophagosome biogenesis. Autophagy 2012; 8:780-93; PMID:22622160; http://dx.doi.org/10.4161/auto.19385

[33] Nakatogawa H, Ishii J, Asai E, Ohsumi Y. Atg4 recycles inappropriately lipidated Atg8 to promote autophagosome biogenesis. Autophagy 2012; 8:177-86; PMID:22240591; http://dx.doi.org/10.4161/auto.8.2.18373

[34] Yu ZQ, Ni T, Hong B, Wang HY, Jiang FJ, Zou S, Chen Y, Zheng XL, Klionsky DJ, Liang Y, et al. Dual roles of Atg8-PE deconjugation by Atg4 in autophagy. Autophagy 2012; 8:883-92; PMID:22652539; http://dx.doi.org/10.4161/auto.19652

[35] Scherz-Shouval R, Shvets E, Fass E, Shorer H, Gil L, Elazar Z. Reactive oxygen species are essential for autophagy and specifically regulate the activity of Atg4. Embo J 2007; 26:1749-60; PMID:17347651; http://dx.doi.org/10.1038/sj.emboj.7601623

[36] Fujita N, Hayashi-Nishino M, Fukumoto H, Omori H, Yamamoto A, Noda T, Yoshimori T. An Atg4B mutant hampers the lipidation of LC3 paralogues and causes defects in autophagosome closure. Mol Biol Cell 2008; 19:4651-9; PMID:18768752; http://dx.doi.org/10.1091/mbc.E08-03-0312

[37] Satoo K, Noda NN, Kumeta H, Fujioka Y, Mizushima N, Ohsumi Y, Inagaki F. The structure of Atg4B-LC3 complex reveals the mechanism of LC3 processing and delipidation during autophagy. EMBO J 2009; 28:1341-50; PMID:19322194; http://dx.doi.org/10.1038/emboj.2009.80

[38] Kalvari I, Tsompanis S, Mulakkal NC, Osgood R, Johansen T, Nezis IP, Promponas VJ. iLIR: A web resource for prediction of Atg8-family interacting proteins. Autophagy 2014; 10:913-25; PMID:24589857; http://dx.doi.org/10.4161/auto.28260

[39] Xue B, Dunbrack RL, Williams RW, Dunker AK, Uversky VN. PONDR-FIT: a meta-predictor of intrinsically disordered amino acids. Biochim Biophys Acta 2010; 1804:996-1010; PMID:20100603; http://dx.doi.org/10.1016/j.bbapap.2010.01.011

[40] Rozenknop A, Rogov VV, Rogova NY, Lohr F, Guntert P, Dikic I, Dotsch V. Characterization of the interaction of GABARAPL-1 with the LIR motif of NBR1. J Mol Biol 2011; 410:477-87; PMID:21620860; http://dx.doi.org/10.1016/j.jmb.2011.05.003

[41] Yang Z, Wilkie-Grantham RP, Yanagi T, Shu CW, Matsuzawa S, Reed JC. ATG4B (Autophagin-1) phosphorylation modulates autophagy. J Biol Chem 2015; 290:26549-61; PMID:26378241; http://dx.doi.org/10.1074/jbc.M115.658088

[42] Rogov VV, Suzuki H, Fiskin E, Wild P, Kniss A, Rozenknop A, Kato R, Kawasaki M, McEwan DG, Lohr F, et al. Structural basis for phosphorylation-triggered autophagic clearance of Salmonella. Biochem J 2013; 454:459-66; PMID:23805866; http://dx.doi.org/10.1042/BJ20121907

[43] Marino G, Fernandez AF, Cabrera S, Lundberg YW, Cabanillas R, Rodriguez F, Salvador-Montoliu N, Vega JA, Germana A, Fueyo A, et al. Autophagy is essential for mouse sense of balance. J Clin Invest 2010; 120:2331-44; PMID:20577052; http://dx.doi.org/10.1172/JCI42601

[44] Ketteler R, Sun Z, Kovacs KF, He WW, Seed B. A pathway sensor for genome-wide screens of intracellular proteolytic cleavage. Genome Biol 2008; 9:R64; PMID:18387192; http://dx.doi.org/10.1186/gb-2008-9-4-r64

[45] Joachim J, Jefferies HB, Razi M, Frith D, Snijders AP, Chakravarty P, Judith D, Tooze SA. Activation of ULK kinase and autophagy by GABARAP trafficking from the centrosome is regulated by WAC and GM130. Mol Cell 2015; 60:899-913; PMID:26687599; http://dx.doi.org/10.1016/j.molcel.2015.11.018

[46] Frey S, Gorlich D. The Xenopus laevis Atg4B Protease: Insights into substrate recognition and application for tag removal from proteins expressed in Pro- and Eukaryotic hosts. PloS One 2015; 10:e0125099; PMID:25923686; http://dx.doi.org/10.1371/journal.pone.0125099

[47] Manil-Segalen M, Lefebvre C, Jenzer C, Trichet M, Boulogne C, Satiat-Jeunemaitre B, Legouis R. The C. elegans LC3 acts downstream of GABARAP to degrade autophagosomes by interacting with the HOPS subunit VPS39. Dev Cell 2014; 28:43-55; PMID:24374177; http://dx.doi.org/10.1016/j.devcel.2013.11.022

[48] Wu F, Watanabe Y, Guo XY, Qi X, Wang P, Zhao HY, Wang Z, Fujioka Y, Zhang H, Ren JQ, et al. Structural Basis of the Differential Function of the Two C. elegans Atg8 Homologs, LGG-1 and LGG-2,

in Autophagy. Mol Cell 2015; 60:914-29; PMID:26687600; http://dx.doi.org/10.1016/j.molcel.2015.11.019

[49] McKnight NC, Jefferies HB, Alemu EA, Saunders RE, Howell M, Johansen T, Tooze SA. Genome-wide siRNA screen reveals amino acid starvation-induced autophagy requires SCOC and WAC. EMBO J 2012; 31:1931-46; PMID:22354037; http://dx.doi.org/10.1038/emboj.2012.36

[50] Kramer RM, Roberts EF, Um SL, Borsch-Haubold AG, Watson SP, Fisher MJ, Jakubowski JA. p38 mitogen-activated protein kinase phosphorylates cytosolic phospholipase A2 (cPLA2) in thrombin-stimulated platelets. Evidence that proline-directed phosphorylation is not required for mobilization of arachidonic acid by cPLA2. J Biol Chem 1996; 271:27723-9; PMID:8910365; http://dx.doi.org/10.1074/jbc.271.44.27723

[51] Winter G, Lobley CM, Prince SM. Decision making in xia2. Acta Crystallogr D Biol Crystallogr 2013; 69:1260-73; PMID:23793152; http://dx.doi.org/10.1107/S0907444913015308

[52] McCoy AJ, Grosse-Kunstleve RW, Adams PD, Winn MD, Storoni LC, Read RJ. Phaser crystallographic software. J Appl Crystallogr 2007; 40:658-74; PMID:19461840; http://dx.doi.org/10.1107/S0021889807021206

[53] Adams PD, Afonine PV, Bunkoczi G, Chen VB, Davis IW, Echols N, Headd JJ, Hung LW, Kapral GJ, Grosse-Kunstleve RW, et al. PHENIX: a comprehensive Python-based system for macromolecular structure solution. Acta Crystallogr D Biol Crystallogr 2010; 66:213-21; PMID:20124702; http://dx.doi.org/10.1107/S0907444909052925

[54] Emsley P, Lohkamp B, Scott WG, Cowtan K. Features and development of Coot. Acta Crystallogr D Biol Crystallogr 2010; 66:486-501; PMID:20383002; http://dx.doi.org/10.1107/S0907444910007493

[55] Vaguine AA, Richelle J, Wodak SJ. SFCHECK: a unified set of procedures for evaluating the quality of macromolecular structure-factor data and their agreement with the atomic model. Acta Crystallogr D Biol Crystallogr 1999; 55:191-205; PMID:10089410; http://dx.doi.org/10.1107/S0907444998006684

[56] Robert X, Gouet P. Deciphering key features in protein structures with the new ENDscript server. Nucleic Acids Res 2014; 42:W320-4; PMID:24753421; http://dx.doi.org/10.1093/nar/gku316